



Unlocking the potential of higher-molecular-weight 5-HT₇R ligands: Synthesis, affinity, and ADMET examination

Patryk Pyka^{a,b,1}, Sabrina Garbo^{c,1}, Aleksandra Murzyn^d, Grzegorz Satała^d, Artur Janusz^e, Michał Górka^e, Wojciech Pietruś^g, Filip Mituła^e, Delfina Popiel^e, Maciej Wieczorek^{e,f}, Biagio Palmisano^c, Alessia Raucci^h, Andrzej J. Bojarski^d, Clemens Zwergel^{h,i}, Ewa Szymańska^a, Katarzyna Kucwaj-Brysz^a, Cecilia Battistelli^{c,*}, Jadwiga Handzlik^{a,*}, Sabina Podlewska^{d,*}

^a Department of Technology and Biotechnology of Drugs, Faculty of Pharmacy, Jagiellonian University, Medical College, Medyczna 9, PL 30-688 Kraków, Poland

^b Doctoral School of Medical and Health Sciences, Jagiellonian University Medical College, 31-530 Kraków, Poland

^c Department of Molecular Medicine, Sapienza University of Rome, Viale Regina Elena 324, 00161, Rome

^d Maj Institute of Pharmacology Polish Academy of Sciences, Smetna 12, 31-343 Kraków, Poland

^e Preclinical Development Department, Celon Pharma S.A., R&D Centre, Marymoncka 15, 05-152 Kaziu Nowy, Poland

^f Clinical Development Department, Celon Pharma S.A., R&D Centre, Marymoncka 15, 05-152 Kaziu Nowy, Poland

^g Medicinal Chemistry Department, Celon Pharma S.A., R&D Centre, Marymoncka 15, 05-152 Kaziu Nowy, Poland

^h Department of Drug Chemistry and Technologies, Sapienza University of Rome, Piazzale Aldo Moro 5, 00185 Rome, Italy

ⁱ Division of Bioorganic Chemistry, School of Pharmacy, Saarland University, Campus B 2.1, D-66123 Saarbrücken, Germany

ARTICLE INFO

Keywords:

Serotonin receptor 5-HT₇
G protein-coupled receptors
ADMET properties
Docking
Molecular modelling
in vitro experiments
MTS assay
Gene expression assay

ABSTRACT

An increasing number of drugs introduced to the market and numerous repositories of compounds with confirmed activity have posed the need to revalidate the state-of-the-art rules that determine the ranges of properties the compounds should possess to become future drugs. In this study, we designed a series of two chemotypes of aryl-piperazine hydantoin ligands of 5-HT₇R, an attractive target in search for innovative CNS drugs, with higher molecular weight (close to or over 500). Consequently, 14 new compounds were synthesised and screened for their receptor activity accompanied by extensive docking studies to evaluate the observed structure–activity/properties relationships. The ADMET characterisation in terms of the biological membrane permeability, metabolic stability, hepatotoxicity, cardiotoxicity, and protein plasma binding of the obtained compounds was carried out *in vitro*. The outcome of these studies constituted the basis for the comprehensive challenge of computational tools for ADMET properties prediction. All the compounds possessed high affinity to the 5-HT₇R (K_i below 250 nM for all analysed structures) with good selectivity over 5-HT₆R and varying affinity towards 5-HT_{2A}R, 5-HT_{1A}R and D₂R. For the best compounds of this study, the expression profile of genes associated with neurodegeneration, anti-oxidant response and anti-inflammatory function was determined, and the survival of the cells (SH-SY5Y as an *in vitro* model of Alzheimer's disease) was evaluated. One 5-HT₇R agent (32) was characterised by a very promising ADMET profile, i.e. good membrane permeability, low hepatotoxicity and cardiotoxicity, and high metabolic stability with the simultaneous high rate of plasma protein binding and high selectivity over other GPCRs considered, together with satisfying gene expression profile modulations and neural cell survival. Such encouraging properties make it a good candidate for further testing and optimisation as a potential agent in the treatment of CNS-related disorders.

1. Introduction

The drug design process is challenged by two significant obstacles:

high costs and long duration. In the quest to improve the success rate of drug searching campaigns, there is constant work on developing various rules and computational protocols for the initial assessment of the

* Corresponding authors.

E-mail addresses: cecilia.battistelli@uniroma1.it (C. Battistelli), j.handzlik@uj.edu.pl (J. Handzlik), smusz@if-pan.krakow.pl (S. Podlewska).

¹ Equal contribution

<https://doi.org/10.1016/j.bioorg.2024.107668>

Received 20 May 2024; Received in revised form 10 July 2024; Accepted 22 July 2024

Available online 24 July 2024

0045-2068/© 2024 The Author(s). Published by Elsevier Inc. This is an open access article under the CC BY license (<http://creativecommons.org/licenses/by/4.0/>).

Table 1
Comparison of the most popular drug-likeness filters.

Filter	Rules
Lipinski [1]	MW<500, logP<5, HBD≤5, HBA≤10
Veber [2]	total polar surface area (TPSA) ≤ 140 Å ² , number of rotatable bonds ≤ 10
Ghose [3]	160 < MW < 480, −0.4 < logP < 5.6, 20 < number of atoms < 70, 40 < molar refractivity < 130
Oprea [4]	HBD<2, 2 < HBA<10, 2 < rotatable bonds < 8, 1 < number of rings < 4
Egan [5]	logP≤5.88, TPSA≤131.6 Å ²

potential drug candidates. One of the most popular solutions is Lipinski's Rule of 5 [1], formulated by Christopher A. Lipinski, which specifies the following features that should be possessed by a prospective orally administered drug: molecular weight (MW) lower than 500, logP below 5 and inclusion in the compound structure of no more than 5 hydrogen bond donors (HBD) and no more than 10 hydrogen bond acceptors (HBA). Other popular drug-likeness filters include the Veber filter [2], Ghose filter [3], Oprea rules [4], Egan rules [5], and the more recent Quantitative Estimate of Druglikeness (QED [6]) or CNS-MPO (a drug-likeness central nervous system multiparameter optimisation [7] with no sharp thresholds, but most preferable MW below 360). Specification of the most popular rules is gathered in Table 1.

The filters mentioned above are often used in the first stages of virtual screening campaigns to quickly remove compounds with unwanted properties. However, these filters should be applied with caution as structural knowledge and consideration of chameleonic properties in drug design should be considered regarding the chemical space beyond the rule of 5 [8,9]. In the subsequent stages, the compound libraries are assessed regarding their activity towards considered targets and/or physicochemical and Absorption, Distribution, Metabolism, Excretion, and Toxicity (ADMET) properties [10,11]. The latter evaluation is not less important than providing the desired compound activity, as unfavourable physicochemical and ADMET profiles can greatly hinder compound's potential as a successful drug [12]. Adequate physicochemistry (solubility, acidity, polarity, etc.), as well as compound efficient absorption and distribution in the body, proper modification by the metabolising enzymes in the body, quick excretion and low toxicity,

are key factors which must be considered during the drug development process. Thus, 5 properties: permeability through biological membranes, cardiotoxicity, metabolic stability, hepatotoxicity and plasma protein binding (PPB), are under particular interest in the early stages of drug R&D. Ability to cross biological barriers is essential for proper compound absorption and distribution throughout the body and for reaching dedicated target [13]. Drug distribution, tissue penetration rate, and pharmacokinetics are also influenced by the rate of PPB. Out of several plasma proteins, human serum albumin (HSA) and α 1-acid glycoprotein (AGP) are the most important [14].

A drug candidate should also not display any sign of cardiotoxicity, often linked to the unwanted blockage of the hERG potassium channels. Compound-induced hepatotoxicity is another serious concern for new potential drugs, as it can lead to liver damage in the form of acute or chronic disease, and it is the most common cause of drug withdrawal from the market [15]. Furthermore, optimal metabolic stability should provide a balance between the sufficient time for a drug to trigger a desired biological response. Still, at the same time, it should minimise the compound's susceptibility to drug-drug interactions [16].

As computational tools have become increasingly significant in predicting the compound ADMET profile, multiple computational tools have already been developed to facilitate this process. However, their prediction power varies significantly depending on the training set and predictive protocol applied [17].

Among the vast array of drug targets, G protein-coupled receptors (GPCRs) hold an exceptional place, serving as a spot for therapeutic modulation for approximately 35 % of already marketed medications [18]. G-protein-coupled receptors (GPCRs) are a superfamily of receptors that mediate many cellular responses to hormones, neurotransmitters, ions, and photons [19]. Due to their involvement in most vital physiological processes in living organisms, alterations in GPCR functions are linked to many diseases [20,21]. GPCRs are the largest family of membrane proteins with a structure of 7 transmembrane helices linked by three intra- and three extracellular loops [15]. Upon ligand binding, a change of GPCR conformation leads to the activation of G proteins, such as G α s and G α i, which regulate adenylate cyclase or G-protein-coupled receptor kinase (GRK) with subsequent coupling to β -arrestin [19]. Based on their structure, GPCRs can be divided into five families, of which rhodopsin (family A) is the largest and most diverse

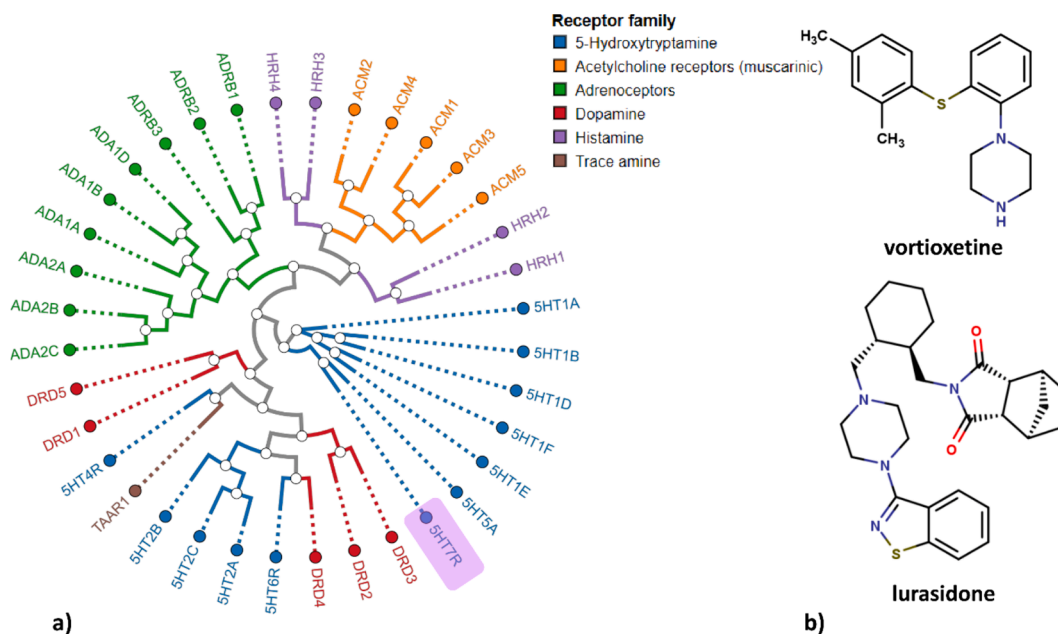


Fig. 1. A) Phylogenetic tree of the aminergic representatives of GPCRs (generated using the GPCRdb tools), B) chemical structures of the most recently approved 5-HT₇R non-selective agents.

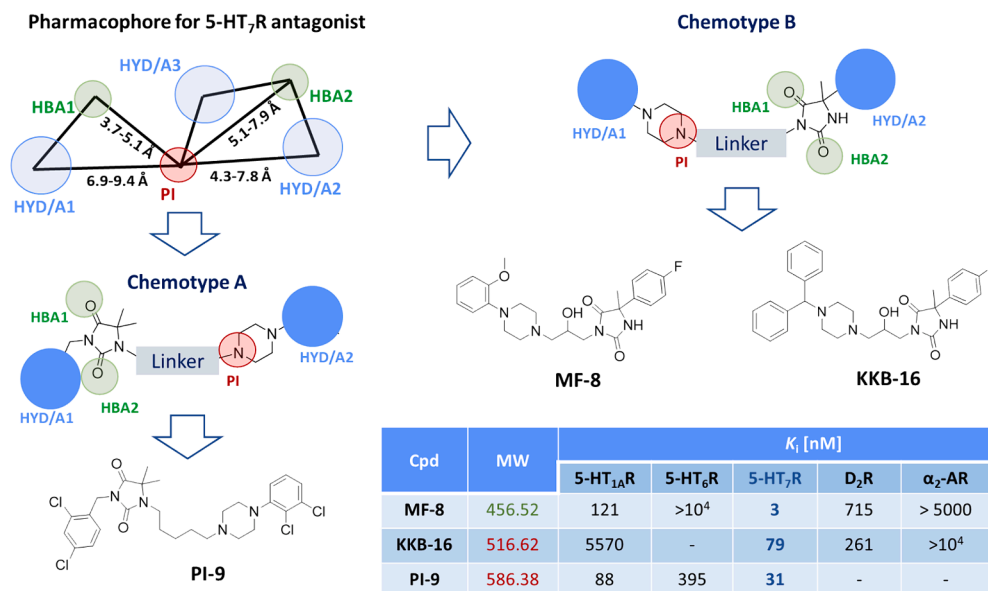


Fig. 2. Pharmacophore model for 5-HT₇R antagonist compared to two chemotypes (A and B) of hydantoin-piperazine ligands found previously. HBA: Hydrogen Bond Acceptor; HYD/A: Hydrophobic/Aromatic; PI: Positive Ionizable moieties. Compound's MW meets (green)/does not meet (red) Lipiński's rule. (For interpretation of the references to colour in this figure legend, the reader is referred to the web version of this article.)

with conserved sequences and, therefore, similar structures and activation mechanisms. Within the rhodopsin family, the aminergic receptors represent an important subgroup. Aminergic GPCRs regulate intracellular signalling pathways via small endogenous biogenic amines (acetylcholine, adrenaline, dopamine, histamine, and serotonin) [22]. In the study, we focused on the serotonin (5-hydroxytryptamine, 5-HT) receptors. Amongst their 14 subtypes, the 5-HT₇R plays a role in various physiological and neurological processes and constitutes an important drug target, as compounds modulating its activity are used to treat depression, cognitive disorders, anxiety and Alzheimer's disease [23]. Flawed signal transduction within this receptor subtype is also associated with disorders of gastrointestinal peristaltic activity [24], cardiovascular reflexes [25], inflammation or epilepsy [26]. Despite more than 20 years of efforts in search for 5-HT₇R selective drugs, none has reached the pharmaceutical market yet, and last approved non-selective 5-HT₇R agents, i.e. vortioxetine (antidepressant, 2013) [27] and lurasidone (antipsychotic, 2014) [28] act also on other targets, (e.g. receptors: 5-HT_{1A}, 5-HT_{1B}, 5-HT₃, D₂ or SERT, respectively) and are assigned with various side effects, like nausea, vomiting, constipation and sexual dysfunction as well as suicide, bleeding or mania. Thus, searching for new potent, selective and "drug-like" 5-HT₇R ligands is still challenging for current medicinal chemistry. Fig. 1 presents the phylogenetic tree of the aminergic representatives of class A GPCRs (generated using the GPCRdb repository) [29], together with the structures of the latest approved non-selective 5-HT₇R agents.

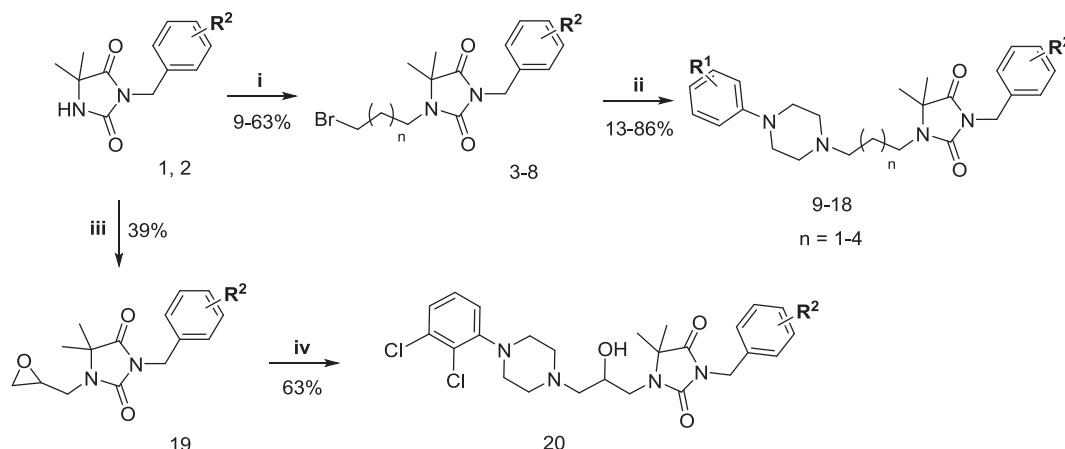
In our previous studies, we have found various hydantoin-piperazine derivatives acting as 5-HT₇R ligands with moderate to significant selectivity over other GPCR targets [30–33]. SAR analysis indicated that the topology of substituents at the hydantoin core and linkers type are responsible for potency and selectivity towards 5-HT₇R. Two chemotypes were particularly interesting (A and B, Fig. 2).

The representatives of both chemotypes meet the requirements of pharmacophore features of 5-HT₇R antagonists [34], but only some members of B (MF-8 and KKB-16) displayed potent affinity and significant selectivity towards 5-HT₇R, while chemotype A was rather not selective (PI-9). Among those compounds, MF-8 emerged as the most potent and selective 5-HT₇R antagonist with marked affinity and substantial selectivity over 5-HT₆R, D₂R, 5-HT_{1A}R, and adrenergic receptors [31,35,36]. The "hit" (MF-8) was used as a lead structure for extended modifications that provided a series of more than 40 new compounds,

but none displayed more beneficial receptor profiles [30,33,35,36]. However, the modifications were also limited via "drug-likeness", and somewhat lower mass of the substituents at piperazine moiety were considered. In contrast, based on pharmacophore requirements, bulky hydrophobic/aromatic (HYD/A) substituents within the aryl part of the arylpiperazine moiety should be profitable for the 5-HT₇R affinity. Among the previous series, the benzhydryl analogue of MF-8, named KKB-16, although doubtful concerning drug-likeness due to its molar mass > 500, turned out to have significantly favourable ADMET parameters *in vitro*, in particular the metabolic stability, clearance and *t*_{1/2}, which resulted in a robust antidepressant-like effect in the rat model, at a dose as low as 0.63 mg/kg [36].

Those results, indicating clear benefits of a "heavy substituent" for both the receptor profile and, controversially, the ADMET profile *in vitro*, drew our particular attention to the issue of the drug-like rule-recommended molecule weight limit in the group of 5-HT₇R antagonists with expected therapeutic effects. In this context, based on the two chemotypes (A and B), new hydantoin-piperazine compounds, in the majority of which the MW exceeds 500, were designed in this study to verify the importance of MW on their activity and selected ADMET properties using both computer-aided and experimental approaches. This study follows the trend of discovering new drug candidates, breaking the traditional rule of 5 [8,9].

Thus, we investigated a series of 14 new 5-HT₇R ligands (concerning chemotypes A and B), which involved the strategic design and synthesis of compounds with exceptional 5-HT₇R activity and selectivity based on our previous studies regarding hydantoin derivatives [30–33]. Considering the potential occurrences of the important interactions coming from the phenyl rings of both piperazine and hydantoin sides, we examined the influence of the series of phenyl ring substitutions on the ligand 5-HT₇R affinity. Taking into account the less favourable 5-HT₇R profile, including the lack of selectivity of earlier representatives of chemotype A, this chemotype was subjected to broader modifications, referring to the likely favourable structural features of chemotype B. In more detail, modifications of PI-9 to maintain the highly hydrophobic chlorine substitutions at the phenyl ring of phenylpiperazine or, with respect to MF-8, replacing it with a 2-methoxy moiety and its bioisosteric analogue, i.e. 2-CN were performed. By varying the linker length (C3–C6) and the introduction of a hydroxyl group (in correspondence to chemotype B) within the compounds of chemotype A, we



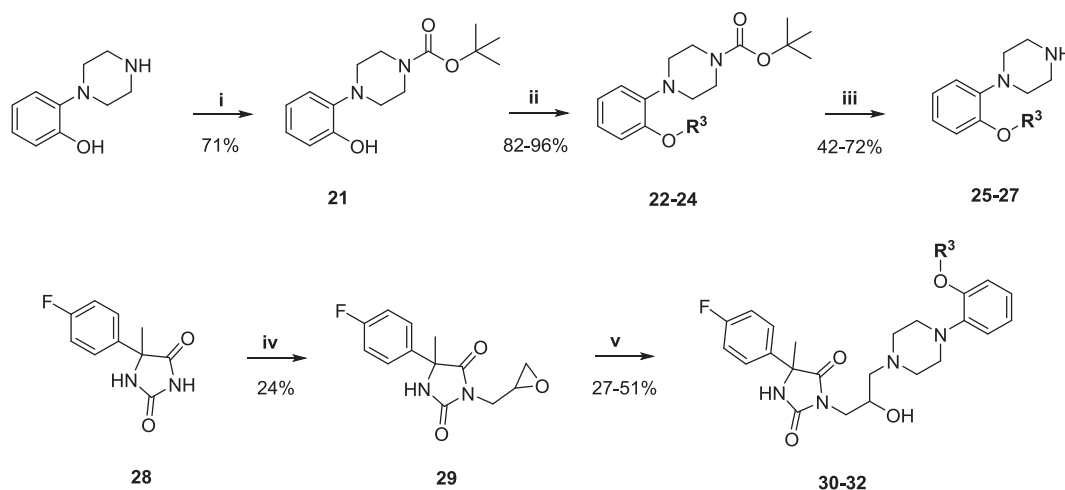
Scheme 1. The synthesis route for compounds of group A (9–18, 20). i) appropriate dibromoalkyl, K₂CO₃, TEBA, acetone, rt; ii) derivative of arylpiperazine, K₂CO₃, acetone, rt; iii) epichlorohydrin, K₂CO₃, TEBA, acetone, rt; iv) 2,3-dichlorophenyl piperazine, μ W.

aimed to preserve the 5-HT₇R activity and improve selectivity over the other GPCRs. On the other hand, for the chemotype B, which was characterised by a more favourable receptor profile, including selectivity to the 5-HT₇R receptor, only modifications of the alkoxy substitution at phenylpiperazine were planned, i.e. an extension of the alkyl 2-MeO moiety of **MF-8** into *i*-Bu, naphthyl- or alkylamine ones. Thus, we intended to introduce substituents, which aimed to increase the lipophilicity of HYD/A1 (Fig. 2) and, in this way, at the same time to increase the affinity for 5-HT₇R and improve the ADMET profile by finding a structural optimum between **MF-8** and **KKB-16**.

The compounds were synthesised and evaluated in *in vitro* experiments on 5-HT₇R affinity and selectivity over 5-HT_{1A}R, 5-HT_{2A}R, 5-HT₆R and D₂R. Next, docking studies were performed to explain the observed structure–activity relationships towards 5-HT₇R and the off-targets, including other GPCRs, hERG potassium channel, and HSA. Comprehensive *in silico* as well as experimental ADMET profile investigations allowed us to evaluate the reliability of predicting the compound's ADMET profile through the described algorithms. In more detail, we performed a comprehensive examination of several *in silico* approaches, confronting their output with the obtained experimental data. In the final step, we delved into the impact of selected active compounds (30–32) on the expression of specific genes in SH-SY5Y cells to provide an in-depth understanding of their potential therapeutic benefits. Specifically, we focused on beta-site amyloid precursor protein cleaving enzyme 1 (BACE-1) [37], an enzyme responsible for the

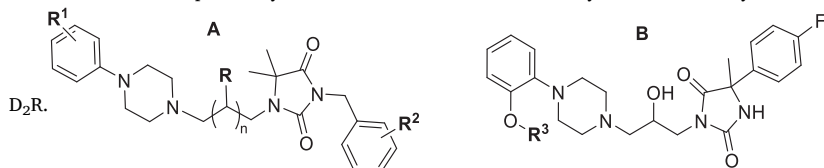
maturation of β -amyloid peptides, whose upregulation is directly associated with Alzheimer's disease. Additionally, we selected antioxidant proteins: haem oxygenase-1 (HO-1) [38], superoxide dismutase (SOD-1) [39], and quinone oxidoreductase-1 (NQO-1) [40] for their collective contribution to cellular protection and redox balance. We also investigated the expression levels of the transcription factors, nuclear factor erythroid 2-related factor 2 (NRF-2) [41] and nuclear factor kappa B (NFkB) [42], for their regulatory roles in antioxidant and pro-inflammatory pathways, respectively. This part of the study aimed to shed light on the regulatory roles of the tested compounds on the expression levels of the considered genes and to explore their potential therapeutic implications. Moreover, related to the explored transcription profile, we also evaluated the proliferation index of the cells in response to the treatments with the intent of deciphering their ability to preserve cell growth.

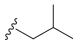
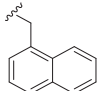
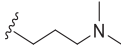
The results of this comprehensive study confirmed the expected benefits, both in terms of the ADMET and receptor profiles for 5-HT₇R ligands with an increased molar mass, exceeding the previously applicable drug similarity rules. They also allowed us to identify particularly favourable “drug-like” properties for one of the representatives of chemotype B, which may constitute an interesting lead structure in the search for an innovative drug with the potential to treat central nervous system disorders, particularly Alzheimer's disease.



Scheme 2. The synthesis route for compounds of group B (30–32). i) Et₃N, Boc₂O, DCM, 2 h, rt; ii) appropriate alkyl halide, NaH, DMF, 24–48 h, rt; iii) TFA, DCM, 24–48 h, reflux; iv) (±)-epichlorohydrin, NaOH, H₂O, 48 h, rt; v) appropriate piperazine intermediate 25–27, K₂CO₃, IPA, 4 h, reflux.

Structures of the compounds synthesised and examined in the study and their affinity and selectivity to 5-HT₇R with respect to 5-HT₆R, 5-HT_{1A}R, 5-HT_{2A}R, and



9-18, 20				30-32							
Cpd	Gr	N	R	R ¹	R ²	R ³	K _i [nM]				
							5-HT ₇ R	5-HT _{1A} R	5-HT _{2A} R	5-HT ₆ R	D ₂ R
9	A	3	H	2-MeO	2,4-Cl	—	42	32	946	2234	5
10	A	3	H	CN	2,4-Cl	—	57	139	546	2692	17
11	A	2	H	2-MeO	2,4-Cl	—	100	16	368	1347	14
12	A	2	H	3,4-Cl	2,4-Cl	—	132	1729	152	230	64
13	A	1	H	3,4-Cl	2,4-Cl	—	121	3129	694	358	1107
14	A	4	H	2-MeO	4-Cl	—	204	25	369	4528	15
15	A	3	H	H	4-Cl	—	151	318	39	2235	35
16	A	3	H	2-MeO	4-Cl	—	64	47	463	3762	8
17	A	4	H	H	2,4-Cl	—	150	177	374	1081	87
18	A	4	H	3,4-diMe	2,4-Cl	—	228	681	327	380	107
20	A	1	OH	2,3-Cl	2,4-Cl	—	168	1037	2541	1079	591
30	B	—	—	—	—		20	382	3397	5537	280
31	B	—	—	—	—		76	778	446	856	481
32	B	—	—	—	—		178	23,016	86,330	4088	26,190

Cpd	MW	Selectivity index			
		5-HT ₆ RK _i /	5-HT _{1A} RK _i /	5-HT _{2A} RK _i /	D ₂ RK _i /
		5-HT ₇ RK _i	5-HT ₇ RK _i	5-HT ₇ RK _i	5-HT ₇ RK _i
9	547.52	53	1	23	0.1
10	542.51	47	2	10	0.3
11	533.49	13	0	4	0.1
12	572.35	2	13	1	0.5
13	558.33	3	26	6	9
14	527.11	22	0	2	0.1
15	483.05	15	2	0	0.2
16	513.08	59	1	7	0.1
17	531.52	7	1	2	0.6
18	559.58	2	3	1	0.5
20	574.32	6	6	15	3.5
30	498.60	277	19	170	14
31	582.60	11	10	6	6
32	527.64	23	129	485	147

2. Results and discussion

2.1. Synthesis

The final compounds, divided into two groups corresponding to chemotypes (A and B), were obtained by distinct multistep synthetic routes (Schemes 1 and 2) based on methods described in the literature [30–32]. N-alkylation at position 1 was performed using either epichlorohydrin or a suitable dibromoalkane to give intermediates (3–8, 19). The final compounds (9–18, 20) were obtained by two methods: classical synthesis (9–18) or microwave-assisted (μ W) synthesis (20) with commercially available derivatives of arylpiperazines. Compounds of group A were further converted into hydrochloride salts.

Compounds within group B were synthesised by a six-step process starting from 2-hydroxyphenylpiperazine ([Scheme 2](#)). The first step involved Boc-protection (**21**), followed by Williamson ether synthesis (**22–24**). The subsequent reaction with trifluoroacetic acid (TFA) allowed to obtain arylpiperazine derivatives (**25–27**). Final compounds within group B (**30–32**) were obtained from compound **29** as free bases

in the reaction of epoxide ring opening. Synthetic methods for intermediates **1**, **2**, **5-8**, **19**, **28** and **29** were reported previously (see [Supplementary Material](#) for details) [30,33]. Final compounds (**20**, **30-32**) were obtained and screened *in vitro* as racemates.

2.2. Affinity of the synthesized compounds to 5-HT₇R, 5-HT_{1A}R, 5-HT_{2A}R, 5-HT₆R, and D₂R

The binding affinity of the synthesised compounds to the principal receptor, i.e. 5-HT₇R, was evaluated in radioligand binding assays. In addition, off-target interactions of the compounds to the selected GPCRs, including 5-HT_{1A}R, 5-HT_{2A}R, 5-HT₆R, and D₂R, were assessed (Table 2; dose-responses curves referring to all K_i values provided are placed in the Supplementary Material – Figs. S1-S5).

In order to compare the obtained affinity profile of the synthesised compounds with the activity profile of already known ligands of the investigated targets, the distribution of K_i values of ligands deposited in the ChEMBL database [43,44] (Fig. 3) towards considered receptors were prepared, and the activity range of the synthesised compounds was

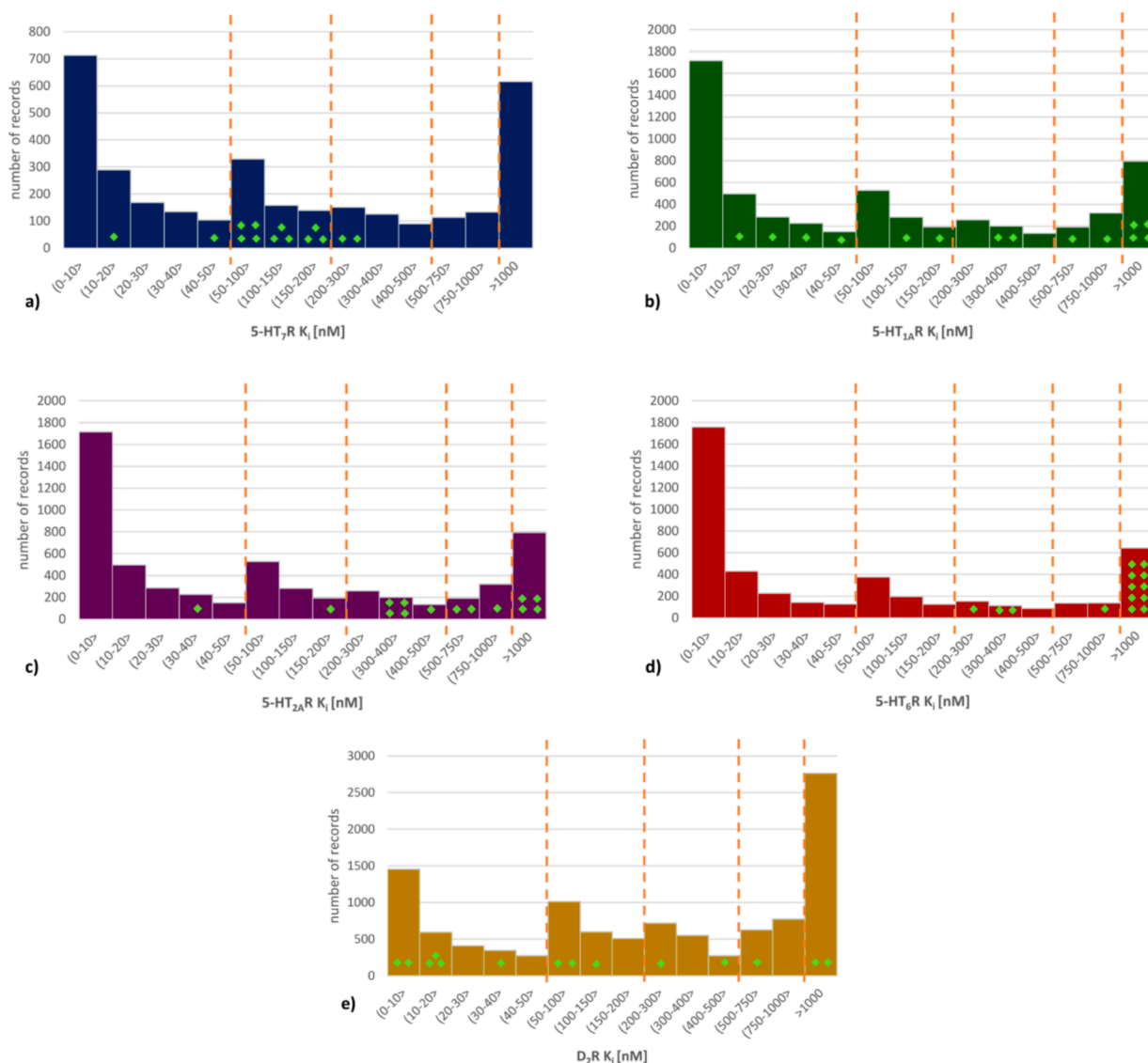


Fig. 3. Histograms of K_i values of compounds deposited in the ChEMBL database with reference to the 5-HT₇, 5-HT_{1A}, 5-HT_{2A}, 5-HT₆, and D₂ receptors. The activity of the synthesised compounds towards respective proteins is marked with green diamonds. (For interpretation of the references to colour in this figure legend, the reader is referred to the web version of this article.)

indicated (Table 1).

The literature data gathered in the ChEMBL database indicate many known ligands of all considered 5-HT receptor subtypes with very good affinity for the respective receptor. In the case of 5-HT₇R, there are 712 records with a K_i value below 10 nM; for comparison, for 5-HT_{1A}R, 5-HT_{2A}R, 5-HT₆R, and D₂R, there are 1715, 1266, 1756, and 1454 of such records, respectively.

The newly synthesised compounds fall into the range of moderate 5-HT₇R activity (one compound with 5-HT₇R K_i below 20 nM, one in the range of 40–50 nM, and 12 compounds with K_i in the range of 50–300 nM, which constitutes a promising starting point for further activity optimisation). On the other hand, for most of them (10 compounds), the 5-HT₆R K_i is higher than 1000 nM, making the reported compounds display good 5-HT₇R/5-HT₆R selectivity. When the 5-HT_{1A}R and 5-HT_{2A}R activity of the synthesised compounds is considered, the results vary depending on the structure. The activity values towards 5-HT_{1A}R range from K_i = 16 nM (for **11**) to K_i exceeding 20 000 nM (for **32**), which makes the most promising compound of this study also a very selective agent towards 5-HT_{1A}R with the 5-HT_{1A}R/5-HT₇R selectivity index equal to 129. Within the group of the synthesised compounds, there are 4 with quite a strong affinity towards 5-HT_{1A}R (5 compounds

with K_i below 100 nM), 6 compounds displaying moderate activity towards this receptor (with K_i values between 100 and 1000 nM), and 4 for which the K_i towards 5-HT_{1A}R was higher than 1000 nM. The K_i values towards 5-HT_{2A}R of all the synthesised compounds were significantly higher compared to 5-HT_{1A}R, with only one compound (**15**) adopting the K_i value below 100 nM (its K_i towards 5-HT_{2A}R was equal to 39 nM). The remaining compounds displayed moderate 5-HT_{2A}R activity (9 compounds with K_i within the range of 100–1000 nM), or they can be classified as non-binders of this receptor (4 compounds with K_i over 1000 nM). The synthesised compound activity was also tested towards the dopamine D₂R. Five compounds displayed very high affinity to D₂R (K_i below 20 nM), including two with K_i below 10 nM. For most compounds, the affinity to D₂R was better than towards 5-HT₇R, leading to D₂R/5-HT₇R selectivity indexes below 1. Only 1 compound (**32**) was characterised by good D₂R/5-HT₇R selectivity with the K_i D₂R/5-HT₇R ratio equal to 147. Compound **32** is also characterised by good selectivity over other 5-HTR subtypes with selectivity indexes over 5-HT_{1A}R, 5-HT_{2A}R, and 5-HT₆R, equal to 129, 51, and 23, respectively.

Examining the results of the affinity for the synthesised compounds to 5-HT₇R in detail, it can be noticed that within the varying linker length among the arylpiperazine, hydantoin and changed substituent at

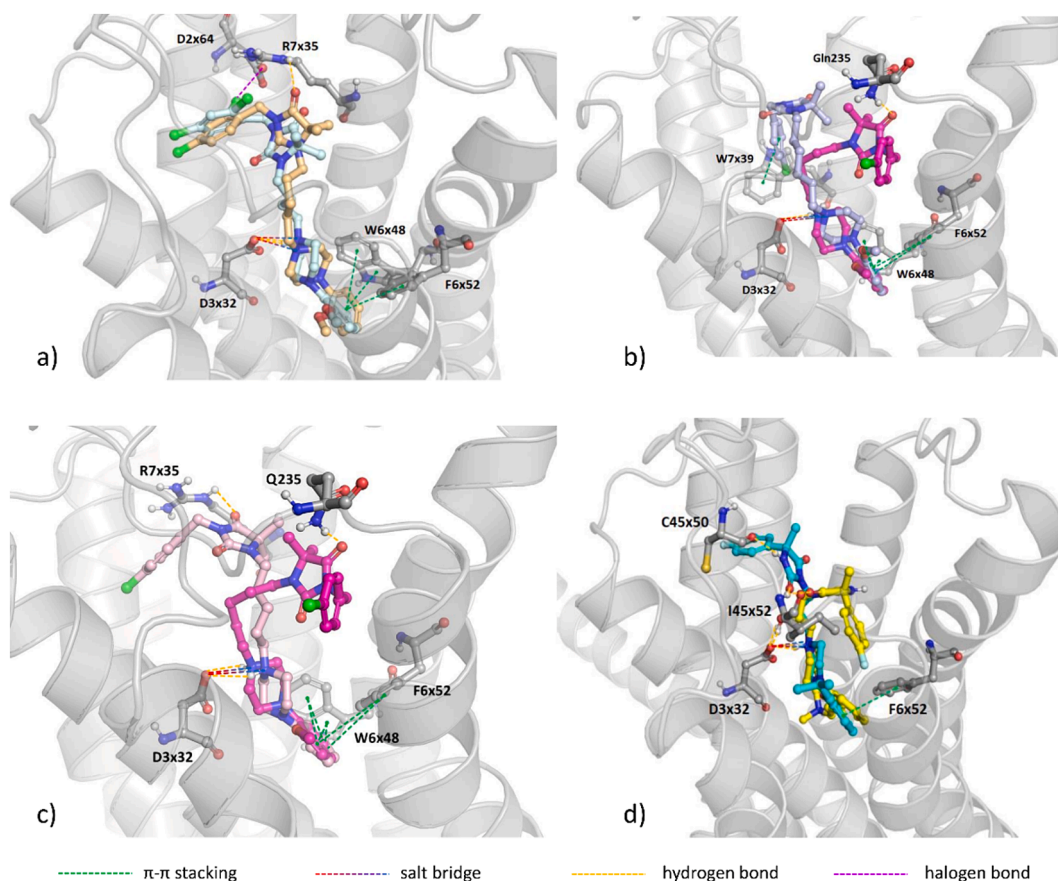


Fig. 4. Comparison of docking poses of selected compound pairs to 5-HT₇R: a) 9 – pale yellow, 11 – light blue, b) 14 – light purple, 16 – magenta, c) 15 – light pink, 16 – magenta, d) 30 – cyan, 32 – yellow. (For interpretation of the references to colour in this figure legend, the reader is referred to the web version of this article.)

the phenyl ring of the arylpiperazine moiety (2,4-diCl substitution of the phenyl ring from the other side of the molecule), the best affinity to the 5-HT₇R was indicated for **9** and **10** (42 and 57 nM respectively). The linker length was equal to 5 for both ligands representing chemotype A, whereas the 2-MeO moiety served as R¹ in **9** and CN in **10**. For comparison, the shortening of the linker by one atom (**11**) resulted in over twice higher K_i value (42 nM for **9** vs. 100 nM for **11**). The 2-MeO substitution and linker of 5 atoms length (**16**) was also the most effective for the 4-chlorophenyl-based structures (**14–16**), with the K_i of 64 nM. Out of compounds of chemotype B (**30–32**), the best 5-HT₇R affinity was observed for **30** (K_i = 20 nM).

The observed experimental outcomes were compared with the *in silico* modelling (selected poses are presented in Fig. 4, and the remaining data are placed in the [Supplementary Material, Fig. S6](#)). For example, compounds **9** and **11**, differentiating from each other only by the length of the linker (Fig. 4), occupy the same region of the 5-HT₇R binding site. Nevertheless, the longer linker of **9** forces slightly different orientations of the hydantoin moiety and the attached dichlorophenyl parts. As a result, the chlorine atoms of **9** form halogen bonds with R7x35 and C45x50, which are not observed for **10** and which probably account for better affinity of **9** in comparison to **10** (K_i = 42 nM vs. K_i = 100 nM, respectively). On the other hand, variations in the length of the linker had a much more significant influence on the pose of **14** and **16**. For these compounds, only the arylpiperazine parts were aligned, forming contacts with W6x48 (π - π stacking) and D3x32 (salt bridge), whereas the position of hydantoin differed significantly. In the case of **16**, it forms a hydrogen bond with I45x52, which can also account for the stronger affinity of these compounds to 5-HT₇R. An analogous case with the presence and absence of the hydrogen bond formed by the hydantoin moiety with I45x52 is observed when the pair of compounds

15 and **16** is compared. When poses of **30** and **32** are compared, the most important difference in the ligand–protein interaction schemes is related to the contacts formed by the hydroxyl group: in the case of **30**, it is a hydrogen bond with T5x40; for **32**, it is a salt bridge with D3x32.

On the other hand, the analysis of the 5-HT₆R activity of the synthesised compounds indicates that compounds **12** and **13** stand out with the K_i values of 230 nM and 358 nM, respectively. These compounds are characterised by both a relatively short linker (C4 or C3, respectively) and substitution of the phenyl ring with two chlorine atoms, which might be a premise for the importance of these features in the increased 5-HT₆R activity. Moderate 5-HT₆R activity was also observed for compound **18** (K_i = 380 nM) with a longer linker, and the arylpiperazine moiety substituted with two methyl residues. Out of the compounds from group B (**30–32**), it was **31**, which displayed the relatively highest 5-HT₆R affinity (K_i = 856 nM); detailed docking data are reported in the [Supplementary Material \(Fig. S9\)](#).

When the results towards 5-HT_{1A}R are analysed, attention should be drawn to compounds **9** and **11**, with the 2-MeO substitution of the phenyl moiety in the arylpiperazine part of the molecule. They vary in the length of the linker, and both display good affinity towards 5-HT_{1A}R (K_i = 32 nM and K_i = 16 nM, respectively). Both **9** and **11** occupy the same position in the receptor's binding pocket and form similar interactions (e.g., salt bridge with D3x32, π - π stacking with phenylalanine residues F6x51 and F6x52). Substitution of the 2-MeO moiety with the nitrile group (as it is in compound **10**) resulted in the change of the orientation of the hydantoin part of the ligand, followed by the absence of the salt bridge with D3x32 and a significant decrease of the 5-HT_{1A}R affinity (K_i = 139 nM). The lowest affinity (K_i = 23016 nM) was recorded for **32**, confirming the very high selectivity of this compound towards 5-HT₇R over 5-HT_{1A}R (complete docking data are available in

Table 3

Summary of the outcome of the experimental verification of ADMET properties of the synthesised compounds.

Cpd	Permeability (P_{app} [10^{-6} cm/s])	Recovery after incubation with Caco-2 cells [%]	hERG inhibition (IC_{50}) [μ M]	hepatotoxicity on HepaRG cell line (IC_{50}) [μ M]	Half-lifetime [min]	Intrinsic clearance (μ L/ min· 10^6 cells)	PPB (fraction bound) [%]
9	0.72	7.8	4.69	35.47	8.96	154.64	97.7
10	0.14	5.0	1.30	34.08	21.05	65.86	97.6
11	1.25	8.4	3.34	35.37	17.67	78.46	95
12	0.00	20.7	1.93	44.17	17.67	78.46	99.4
13	0.00	9.5	6.03	46.94	5.44	255.06	98.4
14	0.72	8.6	2.58	37.95	16.65	83.28	95.9
15	0.63	6.1	10.55	33.65	4.63	299.40	92.8
16	1.58	31.5	2.53	35.73	8.73	158.86	<45
17	0.12	7.5	2.51	33.62	17.32	80.05	61.8
18	0.01	12.9	3.24	34.39	24.16	57.38	96
20	0.00	9.5	11.47	27.54	15.70	88.30	98
30	7.04	52.4	59.89	16.39	24.36	56.91	75
31	0.10	15.4	3.69	9.82	6.94	199.82	45.3
32	6.71	87.5	200.30	>100	stable	0.00	98.1

the [Supplementary Material, Fig. S7](#)).

Discussing the 5-HT_{2A}R structure–activity relationships, it should be pointed out that the best affinity to this receptor displayed compound **15** (K_i = 39 nM), which does not contain a 2-MeO group, in contrast to the structurally similar **14** and **16**. The most selective 5-HT₇R agent (compound **32**) does not display a 5-HT_{2A}R affinity with a selectivity index equal to 485 (detailed docking data of all compounds are reported in the [Supplementary Material, Fig. S8](#)).

Finally, when structure–activity relationships towards D₂R are discussed, all the compounds, but **13** and **32**, display very high D₂R affinity. In the case of **13**, the shorter linker between the hydantoin and arylpiperazine moieties seems to carry the highest responsibility for the activity loss of **13**. On the other hand, when compounds **30–32** are considered, one of the main differences involved the formation of π -cation bonds by **32** due to the structure of the R³ substituent of this ligand (the presence of a protonated amino group). This specific feature of **32** may be the source of the significant decrease in affinity for the D₂ receptor (K_i = 26190 nM) and the increase in the selectivity index value over 5-HT₇R to 147.

In light of the results of combined *in vitro* and *in silico* receptor studies, the topology of chemotype A, despite comprehensive modifications, turned out to be, in general, less favourable for the desired 5-HT₇R selectivity profile. The data indicate an attraction for topology with the phenylpiperazine end at the 3 position of the hydantoin not only for the main target but also for other off-targets, in particular, the D₂R receptor. In contrast, a much higher selectivity towards 5-HT₇R seems to ensure the topology of chemotype B. The receptor profile of 3 representatives (**30–32**) confirms the validity of these modifications, which require further development in order to improve the affinity to 5-HT₇R.

2.3. *In vitro* examination of compound ADMET properties and confrontation with the output of *in silico* tools

Experimental verification of compound ADMET features indicated their promising profile ([Table 3](#)), especially for compound **32**. The assessment of the compound's potential to cross biological membranes indicated significant problems with passing through the Caco-2 barrier (for 10 of the examined compounds, the measured permeability was lower than $1 \cdot 10^{-6}$ cm/s). The highest permeability potential was observed for compounds **30** and **32** with the P_{app} values equal to $7.04 \cdot 10^{-6}$ cm/s and $6.71 \cdot 10^{-6}$ cm/s, respectively). In addition, the amount of compounds present after incubation with Caco-2 cells was determined. For many of them, a significant loss was observed, indicating that the compounds degrade to a large extent in Caco-2 cells or that they may interact with the medium to create a form different enough to be unrecognised by targeted analysis with LC/MS. High recovery (87.5 %) was observed only for **32**.

was observed only for **32**.

Also, when the compounds were assessed in terms of their potential cardiotoxicity (expressed by their potency to block the hERG potassium channel), the lowest affinity to hERG protein was displayed by **32** (IC_{50} = 200.30 μ M), followed by **30** (IC_{50} = 59.89 μ M). On the other end of the spectrum, **10** (IC_{50} = 1.3 μ M) and **12** (IC_{50} = 1.93 μ M) displayed the highest hERG blockage potential among all tested compounds (IC_{50} curves available in the [Supplementary Material, Fig. S11](#)).

The docking studies performed on hERG protein indicated that five of the tested compounds (**9**, **12**, **13**, **16**, **18**) do not form sufficient contacts with amino acid residues in the hERG channel and no valid docking poses were returned for these entities. Most other ligands form π - π stacking interactions within the arylpiperazine moiety, often with Tyr652 residues of different hERG subunits. A distinguishing feature of compounds **10** and **11** is forming a halogen bond within 2,4-dichlorophenyl with Phe C:656 and Ser B:660 residues, respectively. Compounds **20** and **30–32** form one or two hydrogen bonds – the first within the hydroxyl group of the linker and the second associated with the protonated amino group of the hydantoin ring. The notable feature of compound **32** is the formation of additional interactions related to the presence of the protonated tertiary amino group in the arylpiperazine moiety, which includes a hydrogen bond and an additional cation- π bond with Tyr C:652, which is the premise for its ability to block the hERG channel, which was not confirmed in the *in vitro* studies (detailed docking data are reported in the [Supplementary Material, Fig. S12](#)).

Exposure of the HepaRG cell to the synthesised compounds (verifying their hepatotoxicity) indicated dose-dependent toxicity, as the cell viability decreased significantly only at the highest compound concentrations. Compound **32** is an exception, as even at the highest concentrations tested, it did not cause any decrease in the hepatic cell viability (respective curves are available in the [Supplementary Material, Fig. S13](#)).

Compound metabolic stability was expressed by two parameters: half-lifetime and intrinsic clearance. Among the tested compounds, **9**, **13**, **14**, **16**, and **31** showed the lowest stability in the presence of human hepatocytes. On the other hand, **32** stood out as remarkably stable and remained unaffected when incubated with human hepatocytes.

As a last parameter, we examined the binding capabilities of the compounds to HSA. In this case, most compounds (11 out of 14 examined) presented a % bound fraction of more than 95 %. Especially, compound **32**, being of particular interest due to its advantageous ADMET profile, was bound at 98 % to HSA. However, this high fraction of bound compound does not exclude **32** from further development as a future drug, as unbound plasma concentration is determined not by PPB but by hepatic intrinsic clearance after oral dose [45]. A high rate of plasma protein binding facilitates compound transport, and as the binding to HSA is non-covalent, it can be reversed, resulting in an

Table 4

The set of tools used to predict ADMET properties was considered in the study.

Tools	Predicted parameters	Website
ADMETlab 2.0 [46]	Physicochemical properties, druglikeness, pharmacokinetic properties (absorption, distribution, excretion), metabolism (selected CYP's substrate/inhibition), toxicity	https://admetmesh.scbdd.com/
SwissADME [53]	Physicochemical properties, lipophilicity, water solubility, pharmacokinetic properties (GI absorption, BBB permeation, P-gp activity, selected CYP's inhibition, skin permeation), druglikeness, PAINS, Brenk alerts, leadlikeness and synthetic accessibility	http://www.swissadme.ch/
admetSAR [47,48]	Physicochemical properties, water solubility, GI absorption, oral bioavailability, BBB penetration, P-gp activity, pharmacokinetic properties (a.o.: PPB, V _D), selected CYP's activity, toxicity (a.o.: DILI, hERG inhibition, AMES mutagenicity, skin sensitisation)	http://1mmd.ecust.edu.cn/admetSar2/
preADMET [49]	Druglikeness, pharmacokinetic properties (BBB, Caco-2, MDCK and skin permeability, intestinal absorption, PPB), toxicity (Amest test, rodent carcinogenicity assay)	https://preadmet.web.service.bmdrc.org/
pkCSM [50]	Physicochemical properties, lipophilicity, water solubility, pharmacokinetic properties related to absorption, distribution and excretion (a.o.: intestinal absorption, Caco-2 and BBB permeability, fraction unbound, total clearance), metabolism (selected CYP's substrate/inhibition), toxicity	https://biosig/lab/uq.edu.au/pkcsM
Pro-Tox II [54]	Toxicity endpoints (a.o.: acute toxicity, hepatotoxicity, cytotoxicity, carcinogenicity, mutagenicity, immunotoxicity), toxicity targets, toxicity pathways	https://tox-new.ch.arite.de/prottox_II/
pred-hERG 5.0 [56]	Cardiotoxicity (hERG inhibition)	https://predherg.labm.ol.com.br
Cell Line Cytotoxicity Predictor (CLC-Pred) [55]	Cytotoxicity (tumor and non-tumor cell lines)	https://www.way2drug.com/cell-line
DL-DILI prediction server [57]	Hepatotoxicity (Drug-induced Liver Injury)	http://www.pkumdl.cn:8000/DILIserver/DILHome.php https://www.vegahub.eu
VEGA <i>in silico</i> platform 1.2.3 version [51]	Physicochemical properties, toxicity (a.o.: AMES mutagenicity, carcinogenicity, acute toxicity, hepatotoxicity, skin sensitisation, skin and eye irritation, chromosomal aberration, micronucleus assay, estrogen/androgen/thyroid/glucocorticoid receptor effect, NOAEL, LOAEL), environmental toxicity descriptors, lipophilicity, water solubility, pharmacokinetic properties (a.o.: PPB, P-gp activity, skin permeation, T _{1/2})	—
QikProp [52]	Physicochemical properties, structural properties, CNS activity, lipophilicity, water solubility, hERG inhibition, BBB	—

Table 4 (continued)

Tools	Predicted parameters	Website
	penetration, cell membrane permeability, skin permeability, GI absorption, druglikeness	

unbound drug molecule. During further optimisation of **32**, the tissue concentration would need to be determined. On the other hand, **31** and **16** are compounds with the lowest rate of HSA binding (below 50 %), and **30** and **17** displayed moderate rates of HSA binding (75 % and 62 %, respectively); the docking results using the HSA crystal structure are presented in the [Supplementary Material \(Figs. S14–S15\)](#).

The wide range of existing computational tools for ADMET properties assessment faces one important limitation – the ability to evaluate compounds from new chemical space correctly. This problem is partially solved when extensive training datasets are available; however, in most cases, the available experimental data is insufficient to cover the broad chemical space of evaluated ligands. Therefore, we performed a comprehensive assessment of selected tools regarding the correctness of predictions of ADMET properties of the synthesised compounds.

Out of the compared tools, there are several comprehensive packages which enable the characterisation of compounds in terms of a wide range of parameters, but there are also such ones which focus on one selected property. The first group includes online-available tools (ADMETlab 2.0 [46], admetSAR [47,48], preADMET [49], pkCSM [50]), as well as the VEGA platform [51] and QikProp application [52], which enable the determination of a wide range of physicochemical descriptors, drug-likeness and ADMET parameters. Slightly more limited capabilities are provided by the SwissADME service [53], which does not include toxicity prediction of tested compounds. Other tools focus on predicting the cytotoxicity of compounds, considering evaluation against multiple different cell lines (Pro-Tox II [54] and CLC-Pred [55]) or a single type of toxicity, e.g. pred-hERG 5.0 [56] and DL-DILI prediction server [57] (details provided in [Table 4](#)).

2.3.1. Membrane permeability

[Table 5](#) gathers the outcome of the computational assessment of membrane permeability, and the results of *in vitro* tests are included for comparison. A compound's ability to cross biological membranes was usually assessed by predicting its ability to pass through the Caco-2 cells; however, approaches providing the prediction of the outcome of assays based on the mammalian Madin-Darby canine kidney (MDCK) are also available. Most tools provided a quantitative outcome; the admetSAR assessed the compounds qualitatively.

In general, it can be noticed that the computational tools were over-optimistic in evaluating the compound's ability to penetrate biological membranes. ADMETlab 2.0 output mainly contains very high permeability values in the Caco-2 assay and moderate to high permeability in the MDCK assay (ADMETlab 2.0 consistently predicted higher values for the Caco-2 assay outcome than for the MDCK assay). In contrast, higher permeability values were predicted for the MDCK assay compared to Caco-2 by QikProp. The categorical assessment provided by admetSAR concluded that all the compounds would not display permeability via the Caco-2 cells. Although, in general, the predicted absolute values of permeability were the most consistent with the *in vitro* output for the MDCK-based ADMETlab 2.0 predictions, neither this tool nor the other tested approaches were able to capture the structural-permeability dependencies observed in the experimental studies. In particular, it refers to the relatively good permeability of **32** with the simultaneous inability to penetrate the Caco-2 membrane by **12**, **13**, **18**, and **20**. It poses the need to improve further the computational approaches for predicting this property. Particular attention should be paid to their 'resolution' so that for compounds with similar structures, varying predictions can be obtained.

Table 5

The outcome of the predictions of compound membrane permeability using different computational packages (values averaged over all stereoisomers where applicable) and its confrontation with the *in vitro* test results.

Cpd	ADMETlab 2.0		admetSAR	QikProp		preADMET		In vitro results
	Caco-2 [10^{-6} cm/s]	MDCK [10^{-6} cm/s]*	Caco-2	Caco-2 [10^{-6} cm/s]**	MDCK [10^{-6} cm/s]**	Caco-2 [10^{-6} cm/s]	MDCK [10^{-6} cm/s]	Caco-2 [10^{-6} cm/s] (mean)
9	799.83	10.0 (H)	Non-permeable	72.34	153.94	5.53	0.23	0.72 (L)
10	350.75	11.0 (H)	Non-permeable	16.58	30.18	4.66	0.03	0.14 (L)
11	677.64	11.0 (H)	Non-permeable	59.42	148.83	5.49	0.10	1.25 (M)
12	463.45	7.7 (M)	Non-permeable	47.95	672.15	5.61	0.02	0.00 (L)
13	436.52	9.2 (M)	Non-permeable	73.62	480.61	5.58	0.00	0.00 (L)
14	1445.44	10.0 (H)	Non-permeable	62.02	80.48	5.51	0.01	0.72 (L)
15	1061.70	9.8 (H)	Non-permeable	59.90	77.52	5.46	0.18	0.63 (L)
16	1213.39	11.0 (H)	Non-permeable	62.19	50.06	5.46	0.27	1.58 (M)
17	887.16	8.0 (M)	Non-permeable	58.94	111.82	5.57	0.01	0.12 (L)
18	439.54	7.7 (M)	Non-permeable	58.00	160.50	5.58	0.01	0.01 (L)
20	306.20	14.0 (H)	Non-permeable	44.96	365.30	4.46	0.00	0.00 (L)
30	554.63	18.0 (H)	Non-permeable	19.66	17.04	5.34	0.02	7.04 (M)
31	368.98	20.0 (H)	Non-permeable	18.25	15.72	5.45	0.10	0.10 (L)
32	381.94	7.0 (M)	Non-permeable	5.28	4.46	5.48	0.01	6.71 (M)

L- low, M – medium, H- high.

* L, M and H values were assigned by ADMETlab 2.0 web server or the Caco-2 permeability assay protocol, respectively; low: $<2 \times 10^{-6}$ cm/s, medium: $2\text{--}20 \times 10^{-6}$ cm/s, high: $>20 \times 10^{-6}$ cm/s. For Caco-2 permeability (*in vitro* assay): low: $<1 \times 10^{-6}$ cm/s, medium: $1\text{--}10 \times 10^{-6}$ cm/s, high: $>10 \times 10^{-6}$ cm/s.

** values averaged over all stereoisomers.

Table 6

Comparison of the hepatotoxicity predictions obtained using various tools with the *in vitro* test outcome.

Cpd	ADMETlab 2.0		VEGA platform	admetSAR	Pro-Tox II (DILI model)	DL-DILI		In vitro results (IC_{50} [μM])
	Human hepatotoxicity	DILI				prediction	probability	
9	No	Yes	Toxic	Toxic	No	DILI-positive	0.74	35.47
10	Yes	Yes	Toxic	Toxic	No	DILI-positive	0.67	34.08
11	No	Yes	Toxic	Toxic	No	DILI-positive	0.82	35.37
12	No	Yes	Toxic	Toxic	No	DILI-positive	0.85	44.17
13	No	Yes	NON-Toxic	Toxic	No	DILI-positive	0.92	46.94
14	No	Yes	Unknown	Toxic	No	DILI-positive	0.58	37.95
15	No	Yes	Toxic	Toxic	No	DILI-positive	0.57	33.65
16	No	Yes	Toxic	Toxic	No	DILI-positive	0.55	35.73
17	No	Yes	NON-Toxic	Toxic	No	DILI-positive	0.76	33.62
18	No	Yes	NON-Toxic	Toxic	No	DILI-negative	0.43	34.39
20	No	Yes	NON-Toxic	Toxic	No	DILI-positive	0.65	27.54
30	Yes	Yes	Unknown	Toxic	No	DILI-negative	0	16.39
31	Yes	Yes	Unknown	Toxic	No	DILI-negative	0	9.82
32	Yes	No	Unknown	Toxic	No	DILI-negative	0	No influence in the HepaRG cells

2.3.2. Hepatotoxicity

Results of the hepatotoxicity assessment (both computational and experimental) are gathered in Table 6.

In silico assessment of the compounds' hepatotoxic properties was mainly related to predicting whether a compound can induce DILI (Drug-induced Liver Injury). Examination of the obtained predictions revealed that the most accurate hepatotoxicity assessment was provided by the ADMETlab 2.0 (DILI model), as it was the only tool which correctly recognised **32** as a non-hepatotoxic compound with the simultaneous hepatotoxicity indication for the rest of the compound set. In contrast, another model available in this package (Human hepatotoxicity) assessed **32** as toxic (together with **10**, **9**, and **31**). Also, the DL-

DILI method indicated a non-toxicity of **32** (as such, **30** and **31** were also assessed, also displaying lower toxicity than compounds **9–18** and **20**). On the other hand, the usefulness of the VEGA platform, admetSAR, and Pro-Tox II is of limited usage to the evaluation of compounds presented in the study, as they either provided no differentiation between particular structures (the whole set was assessed as toxic or non-toxic), or the hepatotoxicity predictions do not reflect the experimental data, as it has in the case of the VEGA platform output.

2.3.3. Cardiotoxicity

The ability to inhibit hERG potassium channels in cardiomyocytes is the most often used feature for predicting compound cardiotoxicity.

Table 7Comparison of the cardiotoxicity predictions obtained using various tools with the *in vitro* test outcome.

Cpd	ADMETlab 2.0		admetSAR*	QikProp (IC_{50}) [μ M]	pred-hERG 5.0		<i>In vitro</i> results (IC_{50}) [μ M]
	Prediction*	Output value**			Prediction	Categorical potency	
9	Yes	0.995	Yes	0.038	Blocker	Moderate	4.69
10	Yes	0.986	Yes	0.050	Blocker	Moderate	1.30
11	Yes	0.994	Yes	0.215	Blocker	Moderate	3.34
12	Yes	0.987	Yes	0.085	Blocker	Moderate	1.93
13	Yes	0.986	Yes	7.656	Blocker	Moderate	6.03
14	Yes	0.997	Yes	0.028	Blocker	Moderate	2.58
15	Yes	0.989	Yes	0.040	Blocker	Moderate	10.55
16	Yes	0.996	Yes	0.734	Blocker	Moderate	2.53
17	Yes	0.989	Yes	0.026	Blocker	Moderate	2.51
18	Yes	0.978	Yes	0.042	Blocker	Moderate	3.24
20	Yes	0.944	Yes	0.788	Blocker	Moderate	11.47
30	Yes	0.910	Yes	0.050	Blocker	Moderate	59.89
31	Yes	0.955	Yes	0.001	Blocker	Moderate	3.69
32	Yes	0.881	Yes	0.005	Blocker	Moderate	200.30

* Yes – active compound (hERG blocker), No – inactive compound. ** Probability of a molecule to be active towards hERG.

Table 8Comparison of the metabolic stability predictions obtained using various tools with the *in vitro* test outcome.

Cpd	ADMETlab 2.0		VEGA platform	<i>In vitro</i> results	
	$T_{1/2}$ [h]	Clearance [mL/min/kg]		$T_{1/2}$ [min] ([h])	Clearance _{int} (μ L/min \cdot 10 ⁶ cells)
9	0.115	6.90	17.06	8.96 (0.15)	154.64
10	0.07	6.97	16	21.05 (0.35)	65.86
11	0.139	7.17	16.64	17.67 (0.29)	78.46
12	0.039	5.58	121.67	17.67 (0.29)	78.46
13	0.042	5.71	136.23	5.44 (0.09)	255.06
14	0.112	6.66	7.603	16.65 (0.28)	83.28
15	0.115	5.14	8.305	4.63 (0.08)	299.40
16	0.138	6.94	7.617	8.73 (0.15)	158.86
17	0.076	5.46	18.67	17.32 (0.29)	80.05
18	0.044	5.51	23.47	24.16 (0.40)	57.38
20	0.05	7.25	80.77	15.70 (0.26)	88.30
30	0.04	7.45	11	24.36 (0.41)	56.91
31	0.022	8.27	13.34	6.94 (0.12)	199.82
32	0.031	7.39	11.12	stable	0.00

Tools such as ADMETlab 2.0, admetSAR and pred-hERG 5.0 enable categorising tested compounds as blockers or non-blockers, while quantitative data (IC_{50} values) obtained thanks to QikProp allow for comparison of the hERG block potency for individual compounds (Table 7). In similarity to the hepatotoxicity assessment, the approaches which classify compounds as hERG blockers/non-blockers were not useful in the assessment of our compounds, as they returned a consistent answer for the whole compound set (all the compounds were predicted to block the hERG channel without any distinction of **32**, which was characterised by significantly higher IC_{50} in the *in vitro* tests in comparison to the rest of the compounds). On the other hand, when a numerical answer during the hERG blockage assessment is provided, again, the ADMETlab 2.0 managed to distinguish **32** from the rest of the compounds, indicating the lowest probability value to display activity

Table 9Comparison of the PPB predictions obtained using various tools with the *in vitro* test outcome.

Cpd	ADMETlab 2.0 [% of fraction bound]	admetSAR (fraction bound)	preADMET [% of fraction bound]	pkCSM [fu*]	<i>In vitro</i> results [% of fraction bound]
9	95.66	1.014	85.42	0.038	97.7
10	95.73	1.005	84.96	0.050	97.6
11	95.13	1.019	86.03	0.062	95
12	98.34	1.044	84.50	0.030	99.4
13	98.01	1.098	84.66	0.031	98.4
14	94.51	1.033	86.89	0.019	95.9
15	92.79	1.068	85.92	0.072	92.8
16	93.83	1.027	86.36	0.040	<45
17	96.16	1.076	85.27	0.040	61.8
18	97.58	1.015	87.20	0.006	96
20	98.07	1.15	98.34	0.126	98
30	92.11	1.006	84.58	0.093	75
31	98.2	1.105	83.83	0.093	45.3
32	78.43	0.95	21.37	0.212	98.1

*predicted fraction unbound in human (numeric fu).

toward hERG equal to 0.881. Lower values were also returned for the other compounds, for which the hERG_{IC50} adopted higher values: **20** (IC_{50} = 11.47 μ M; the value returned by the ADMETlab2.0: 0.944) and **30** (IC_{50} = 59.89 μ M); the value returned by the ADMETlab2.0: 0.910). QikProp also distinguished between **32** and the rest of the compounds; however, surprisingly, in this case, **32** was the compound for which the predicted IC_{50} was the lowest out of the whole compound set.

2.3.4. Metabolic stability

Similar to the *in vitro* tests, computational tools also enabled the characterisation of compounds in terms of their metabolic stability using different parameters (Table 8). Although, in general, the half-lifetime values predicted by ADMETlab2.0 were significantly closer to the outcome of the *in vitro* tests (in comparison to the $T_{1/2}$ values provided by the VEGA platform), again, we face the problem of the loss of the relationships between more and less stable compounds. In particular, ADMETlab2.0 provided no premise about the potential great stability of **32**, which was revealed by the *in vitro* tests. Similar conclusions can be drawn from the clearance predictions; however, this time, the values provided by ADMETlab 2.0 differed significantly from the outcome of the *in vitro* experiments, and again, the high stability of **32** was not indicated.

2.3.5. Plasma protein binding

The data predicted by the online tools show a similar high ability of

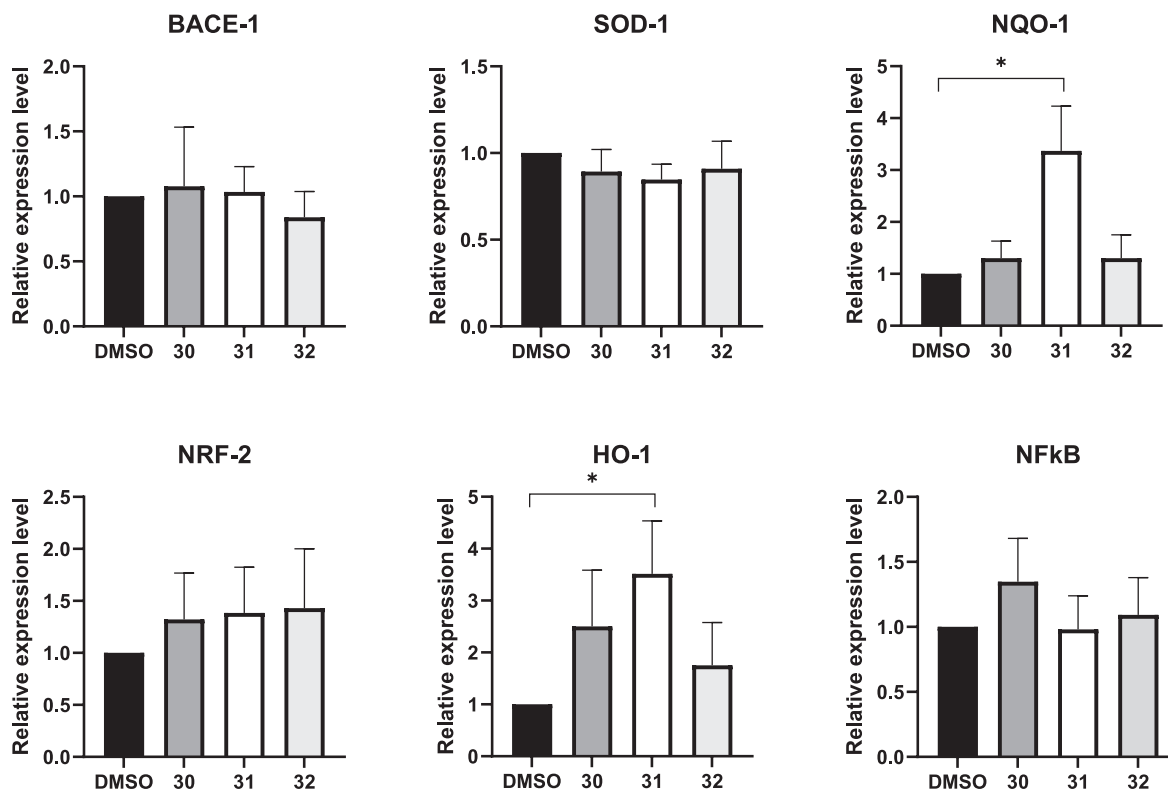


Fig. 5. Qrt-pcr analysis for the indicated transcripts in sh-sy5y treated with the compounds 30, 31 and 32 at 10 μ M for 48 h. DMSO (control) represent the cells treated with the vehicle. The values are calculated by the $2^{(-\Delta Ct)}$ method, expressed as fold of expression vs. the control (arbitrary value = 1) and shown as mean \pm SEM. Statistically significant differences are reported (*, $p < 0.05$) for four independent experiments.

all the tested compounds to bind to plasma proteins (Table 9), which could potentially be unfavourable for their *in vivo* pharmacokinetics. Concurrently, the lowest PPB values were predicted *in silico* for compound 32 by ADMETlab2.0, admetSAR, and preADMET. In general, all the considered computational tools predicted the synthesised compounds to be bound with the plasma proteins in high fraction – the highest binding rate was predicted by ADMETlab2.0 and admetSAR, whereas slightly lower values were predicted for preADMET. Although the PPB rate for 32 was predicted to be the lowest out of all tested compounds, it was not confirmed in the *in vitro* examinations, as the fraction of compound bound to HSA was equal to 98.1 %, indicating the inaccuracy of this *in silico* predictions.

2.4. Neurotoxic/neuroprotective effects in SH-SY5Y cells

Due to the more favourable pharmacological and ADMET profile found for group B, compared to group A, in previous assays *in vitro*, compounds 30, 31, and 32 were selected for additional investigations on their potential neurotoxic/neuroprotective effects in the neuroblastoma SH-SY5Y cell line model. Thus, their impact on gene expression modulation of several mRNAs whose expression is associated with neurodegeneration, oxidative metabolism and inflammation, i.e. BACE-1, HO-1, SOD-1, NQO-1, NRF-2 and NFkB, was investigated in the cells, upon the treatment with compounds at 10 μ M for 48 h. The results highlight a general trend of upregulating the antioxidant genes (HO-1 and NQO-1) in response to the tested compounds 30–32 (Fig. 5).

Compounds 30–32 did not cause any statistically significant changes in the expression of BACE-1, NRF-2 and NFkB genes. These results demonstrate negligible effects of the hydantoin compounds 30–32 on genes associated with both neurodegeneration and inflammation at these concentrations.

Due to those results, the MTS assay was performed to examine the proliferation and viability of SH-SY5Y cells upon the treatment with the

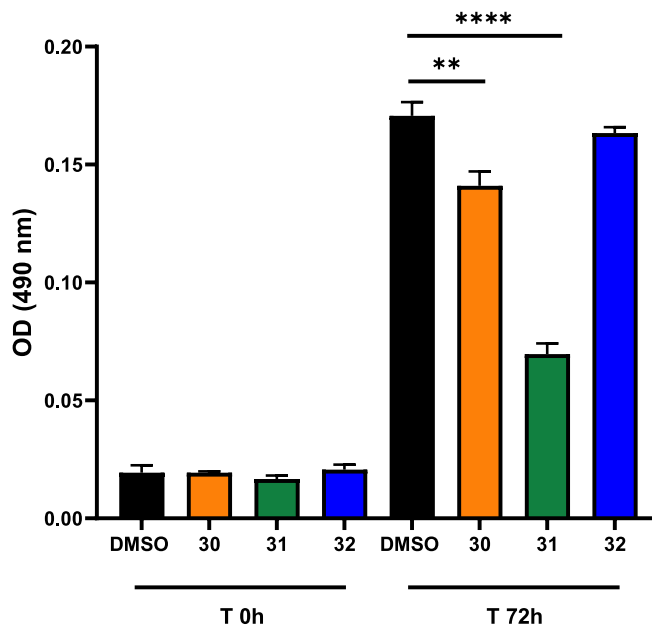


Fig. 6. MTS assay for SH-SY5Y cells proliferation treated with the compounds 30–32 at 10 μ M for 72 h. The values are shown as mean \pm SD. Statistically significant differences are reported (**, $p < 0.01$; ****, $p < 0.0001$).

compounds 30–32 at 10 μ M for 72 h (Fig. 6). The results obtained indicated significant antiproliferative effects for compound 31 and a much weaker one for 30, while compound 32 did not influence the neuroblastoma cell proliferation (Fig. 6). According to the results of the MTS assay, only compound 31 displayed a meaningful risk of neurotoxic

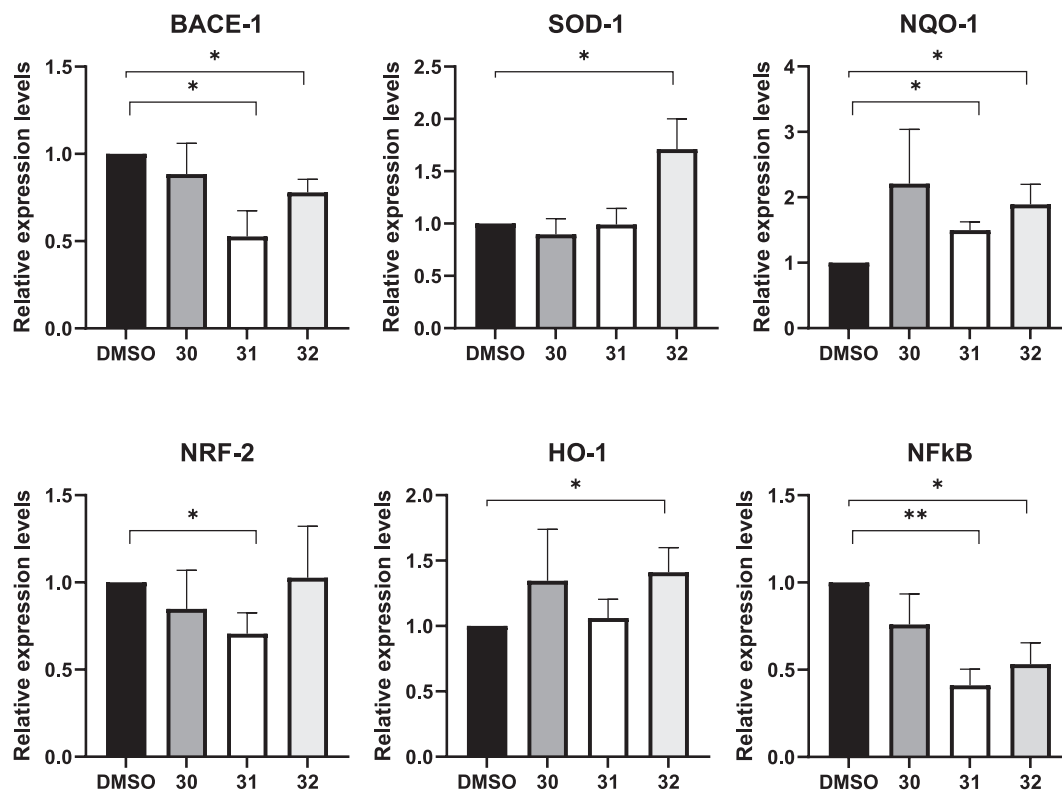


Fig. 7. Qrt-pcr analysis for the indicated transcripts in sh-sy5y treated with the compounds 30, 31 and 32 at 1 μ M for 48 h. DMSO (control) represent the cells treated with the vehicle. The values are calculated by the $2(-\Delta Ct)$ method, expressed as fold of expression vs. the control (arbitrary value = 1) and shown as mean \pm SEM. Statistically significant differences are reported (*, $p < 0.05$; **, $p < 0.01$) for four independent experiments.

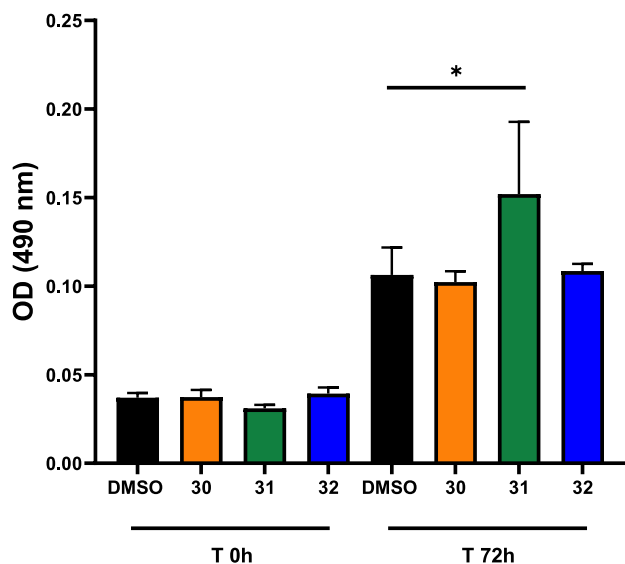


Fig. 8. MTS assay for SH-SY5Y cells proliferation treated with the compounds 30–32 at 1 μ M for 72 h. The values are shown as mean \pm SD. Statistically significant differences are reported (*, $p < 0.05$).

effects, while **32** turned out to be completely safe in terms of the risk of neurotoxicity investigated.

Due to the observed neurotoxic effect of the compounds on cell proliferation, effects of **30–32** were evaluated at a lower concentration, and the same assays were performed on SH-SY5Y cells (Fig. 7).

Notably, the treatments with the compounds at 1 μ M for 48 h positively regulate the expression of the antioxidant genes SOD-1, NQO-1 and HO-1 (induced by compounds **31** and **32**, respectively), while the

expression of BACE-1 (related to Alzheimer's disease development) and NFkB (related to cell inflammation) decreases. Taken together, these data indicate that the treatment with 1 μ M of the tested compounds for 48 h has a significant antioxidant and anti-inflammatory effect. In order to evaluate cell proliferation, an MTS assay was performed in the same experimental conditions (Fig. 8).

The gene expression data result in accordance with those obtained in the proliferation test. Upregulation of some antioxidant genes should increase cell viability, which can be reflected in the proliferation levels observed in response to the treatment with compound **31**.

Overall, compounds **31** and **32** possess the potential to be applied in the treatment of Alzheimer's disease or in the therapy of neuro-inflammation as they regulate genes related to these diseases.

3. Conclusions

Prompted by our previous finding, where the **KKB-16** of higher MW were characterised by favourable ADMET parameters, we successfully designed and synthesised a series of aryl-piperazine 5-HT₇R ligands with higher MW, which did not negatively impact their biological properties. Through comprehensive computational and *in vitro* characterisation of the ADMET properties, we identified compound **32** as a very promising candidate for further testing and optimisation. Moreover, we explored the impact of selected compounds on the expression of specific genes in SH-SY5Y cells, providing an in-depth understanding of their potential therapeutic benefits and usefulness in the search for potential agents that act within the central nervous system and can serve as new drug candidates towards the Alzheimer's disease. Additionally, our extensive study on freely available tools for ADMET features assessment *in silico* allowed us to identify the most valuable tools for evaluating aryl-piperazine-based derivatives, as well as to indicate the limitations of already existing tools and posing the need of further tuning of predictive models related to ADMET properties. Although, in general, the

predictions provided by widely accessible *in silico* tools were not very accurate with the outcome of the *in vitro* studies, it's worth noting that ADMETlab 2.0 was able to correctly distinguish the unique properties of **32** in comparison to the rest of the compound series. However, it only referred to cardiotoxicity and hepatotoxicity, while the other properties were not predicted accurately. Nevertheless, considering the generalizability of ADMETlab 2.0 and the whole range of parameters assessed, it can be used as a screening tool for a very general evaluation of compounds in terms of ADMET properties. On the other hand, the prediction accuracy depends on the similarity of the examples from the training set to the assessed compounds, so it's always worth checking whether our compounds fall into the chemical space covered by the respective training set if there is an option to do so.

Exploring higher-molecular-weight ligands for 5-HT₇R presented in this study is a great example of thinking outside the box and challenging the conventional Lipinski's Rule of Five. Our study's success demonstrates the power of non-standard thinking and encourages the continuation of innovative approaches which can lead to better and more effective drugs.

4. Materials and methods

4.1. Chemistry

¹H NMR and ¹³C NMR spectra were routinely recorded on a Varian Mercury-VX 500 MHz PFG apparatus in DMSO-*d*₆ or CDCl₃. Spectra were carried out at ambient temperature using the solvent signal as an internal standard. Chemical shifts in spectra were reported in parts per million (ppm) on the δ scale with coupling constants (*J*) values in Hertz. Mass spectra were recorded on a UPLC-MS/MS system consisting of a Waters ACQUITY®UPLC® (Waters Corporation, Milford, MA, USA), which is coupled to a Waters TQD mass spectrometer (electrospray ionisation mode ESI-tandem quadrupole). Chromatographic separations were carried out using the Acquity UPLC BEH (bridged ethyl hybrid) C18 column; 2.1 × 100 mm, and 1.7 μ m particle size, equipped with Acquity UPLC BEH C18 VanGuard precolumn (Waters Corporation, Milford, MA, USA); 2.1 × 5 mm, and 1.7 μ m particle size. The column was maintained at 40 °C and eluted under gradient conditions from 95 % to 0 % of eluent A over 10 min, at a flow rate of 0.3 mL·min⁻¹. Eluent A: water/formic acid (0.1 %, v/v); eluent B: acetonitrile/formic acid (0.1 %, v/v). Chromatograms were made using Waters eλ PDA detector. Spectra were analysed in the 200–700 nm range with 1.2 nm resolution and a sampling rate of 20 points/s. MS detection settings of Waters TQD mass spectrometer were as follows: source temperature 150 °C, desolvation temperature 350 °C, desolvation gas flow rate 600 L·h⁻¹, cone gas flow 100 L·h⁻¹, capillary potential 3.00 kV, cone potential 40 V. Nitrogen was used for both nebulising and drying gas. The data were obtained in a scan mode ranging from 50 to 1000 *m/z* in 0.5 s intervals. The data acquisition software was MassLynx V 4.1 (Waters Corporation, Milford, MA, USA). Retention times (*t*_R) are given in minutes. Thin layer chromatography (TLC) was performed on Merck silica gel 60 F254 plates and the spots were visualised by UV light. Melting points (mp) were determined using Mel-Temp II apparatus and were uncorrected. For column chromatography purification, a CombiFlash Rf + apparatus (Teledyne Isco Inc., USA) was used, and the mixture of dichloromethane/methanol (methanol + 1–2 % ammonia) was applied as a mobile phase. High-resolution mass spectra (HR-MS) were recorded on a UPLCMS/MS system consisting of a Waters Acquity I-Class Plus UPLC (Waters Corporation, Milford, MA, USA) coupled to a Waters Synapt XS mass spectrometer (electrospray ionisation mode). Chromatographic separations were carried out using the Acquity UPLC BEH (bridged ethylene hybrid) C18 column, 2.1 × 100 mm, and 1.7 μ m particle size, equipped with an Acquity UPLC BEH C18 VanGuard precolumn; 2.1 × 5 mm, 1.7 μ m particle size. The column temperature was maintained at 40 °C, and the samples were eluted applying a gradient from 95 to 0 % of eluent A and 5 to 100 % of eluent B over 10 min at a flow rate of 0.3 mL

min – 1 (eluent A: water/formic acid (0.1 %, v/v); eluent B: acetonitrile/formic acid (0.1 %, v/v)). Chromatograms were recorded using a Waters eλ PDA detector. Spectra were analysed from 200 to 700 nm with 1.2 nm resolution and a sampling rate of 20 points/s. MS detection settings of the Waters Synapt XS mass spectrometer were as follows: source temperature 150 °C, desolvation temperature 250 °C, desolvation gas flow rate 600 L·h⁻¹, cone gas flow 100 L·h⁻¹, capillary potential 3.00 kV, cone potential 30 V. Nitrogen was used for both nebulising and drying gas. The data were obtained in a scan mode ranging from 50 to 1000 *m/z* in 0.2 s intervals. Leu-enkephalin was used as a mass reference. The data acquisition software was MassLynx V 4.2 (Waters). Compounds **1**, **2** [30], **5** [58], **6**, **7** [30], **8**, **19** [59], **28** and **29** [33] were synthesised according to reported procedures. Intermediates **3–8** were used in crude form for the synthesis of final compounds of chemotype A (see [Supplementary Material](#)).

4.1.1. General procedure for *o*-alkylation of *tert*-butyl 4-(2-hydroxyphenyl)piperazine-1-carboxylate derivatives

Tert-butyl 4-(2-hydroxyphenyl)piperazine-1-carboxylate (4 mmol) was dissolved in 20 mL of DMF in a round bottom flask cooled to 0 °C. Sodium hydride (8 mmol, 2 equiv.) was added in portions to the solution, and the mixture was stirred for 30 min; the alkylating reagent (4.8 mmol, 1.2 equiv.) was then added. The reaction was carried out at room temperature for 24 h. The mixture was extracted with DCM (3x25 mL), and the collected organic layers were washed with brine, dried over anhydrous Na₂SO₄ and densified in vacuo. The desirable product was used directly without further purification (Method A) or purified on flash chromatography with DCM:MeOH (Method B).

Tert-butyl 4-(2-isobutoxyphenyl)piperazine-1-carboxylate (**22**). Method A. Brown oil, yield: 95.7 %. ¹H NMR (500 MHz, DMSO-*d*₆) δ 6.95 – 6.88 (m, 2H), 6.87 – 6.82 (m, 2H), 3.73 (d, *J* = 6.2 Hz, 2H), 3.43 (s, 4H), 2.93 – 2.88 (m, 4H), 2.03 (dp, *J* = 13.0, 6.6 Hz, 1H), 1.41 (s, 9H), 1.00 (d, *J* = 6.7 Hz, 6H). MS (ESI) *m/z* calculated for [M+H]⁺ C₁₉H₃₁N₂O₃ 335.23, found 335.31.

Tert-butyl 4-(2-(naphthalen-1-ylmethoxy)phenyl)piperazine-1-carboxylate (**23**). Method A. Brown oil, yield: 94 %. ¹H NMR (500 MHz, CDCl₃) δ 8.08 (d, *J* = 8.8 Hz, 1H), 7.90 (dd, *J* = 7.5, 1.9 Hz, 1H), 7.86 (d, *J* = 8.2 Hz, 1H), 7.65 (d, *J* = 6.9 Hz, 1H), 7.56 – 7.50 (m, 2H), 7.48 (dd, *J* = 8.2, 7.0 Hz, 1H), 7.11 (d, *J* = 7.8 Hz, 1H), 7.07 – 7.01 (m, 1H), 7.00 – 6.92 (m, 2H), 5.58 (s, 2H), 3.44 (s, 4H), 3.01 (s, 4H), 1.45 (s, 9H). MS (ESI) *m/z* calculated for [M+H]⁺ [C₂₆H₃₁N₂O₃]⁺ 419.23, found 419.31.

Tert-butyl 4-(2-(3-(dimethylamino)propoxy)phenyl)piperazine-1-carboxylate (**24**). Method B. Brown oil, yield: 81.8 %. ¹H NMR (500 MHz, CDCl₃) δ 6.98 (ddd, *J* = 7.9, 6.8, 2.3 Hz, 1H), 6.93 – 6.89 (m, 2H), 6.88 – 6.86 (m, 1H), 4.06 (t, *J* = 6.3 Hz, 2H), 3.61 – 3.57 (m, 4H), 3.03 – 2.98 (m, 4H), 2.54 (t, *J* = 7.4 Hz, 2H), 2.30 (s, 6H), 2.08 – 2.01 (m, 2H), 1.48 (s, 9H). MS (ESI) *m/z* calculated for [M+H]⁺ [C₂₀H₃₄N₃O₃]⁺ 364.26, found 364.35.

4.1.2. General procedure for deprotection of Boc-group

An appropriate Boc-protected arylpiperazine (4 mmol) was dissolved in 8 cm³ of DCM, then TFA (20 mmol, 5 equiv.) was slowly added to the solution, and the reaction was refluxed for 24 h. After this time, the solvents were removed in vacuo, and the pH of the residue was adjusted with a saturated solution of NaHCO₃ to a pH of around 9–10. The mixture was extracted with DCM (4x20 mL). The organic layer was then washed with brine, dried over anhydrous Na₂SO₄ and evaporated. The product was purified by flash chromatography with DCM and 1 % ammonia solution in MeOH.

1-(2-Isobutoxyphenyl)piperazine (**25**). Brown oil, yield: 41.5 %. ¹H NMR (500 MHz, CDCl₃) δ 7.02 – 6.97 (m, 1H), 6.90 (d, *J* = 4.1 Hz, 2H), 6.85 (d, *J* = 7.9 Hz, 1H), 3.76 (dd, *J* = 10.4, 3.7 Hz, 2H), 3.49 – 3.45 (m, 1H), 3.28 (s, 6H), 3.11 (dt, *J* = 9.5, 4.6 Hz, 1H), 2.14 (td, *J* = 13.2, 6.5 Hz, 1H), 1.05 (d, *J* = 6.7 Hz, 6H). MS (ESI) *m/z* calculated for [M+H]⁺ C₁₄H₂₃N₂O 235.18, found 235.30.

1-(2-(Naphthalen-1-ylmethoxy)phenyl)piperazine (**26**). Brown oil,

yield: 69.2 %. ^1H NMR (500 MHz, CDCl_3) δ 8.09 (dd, $J=8.3$, 1.2 Hz, 1H), 7.90 (d, $J=7.2$ Hz, 1H), 7.85 (d, $J=8.3$ Hz, 1H), 7.67 (d, $J=7.0$ Hz, 1H), 7.57–7.50 (m, 2H), 7.50–7.46 (m, 1H), 7.08 (d, $J=7.4$ Hz, 1H), 7.04–6.99 (m, 1H), 6.99–6.96 (m, 2H), 5.58 (s, 2H), 3.08 (s, 4H), 2.98–2.91 (m, 4H). MS (ESI) m/z calculated for $[\text{M}+\text{H}]^+$ $[\text{C}_{21}\text{H}_{23}\text{N}_2\text{O}]^+$ 319.18, found 318.42.

N,N-dimethyl-3-(2-(piperazin-1-yl)phenoxy)propan-1-amine (27). Brown oil, yield: 71.6 %. ^1H NMR (500 MHz, CDCl_3) δ NMR (500 MHz, CDCl_3) δ 6.98–6.93 (m, 1H), 6.91 (d, $J=0.8$ Hz, 1H), 6.91–6.89 (m, 1H), 6.86 (d, $J=7.4$ Hz, 1H), 4.04 (t, $J=6.3$ Hz, 2H), 3.07 (s, 8H), 2.51–2.48 (m, 2H), 2.26 (s, 6H), 2.06–1.97 (m, 2H). MS (ESI) m/z calculated for $[\text{M}+\text{H}]^+$ $[\text{C}_{15}\text{H}_{26}\text{N}_3\text{O}]^+$ 264.21, found 264.27.

4.1.3. General procedure for the synthesis of final compounds within group A (9–18)

To an appropriately substituted phenylpiperazine (4 mmol) dissolved in acetone (15 mL), K_2CO_3 (12 mmol, 4 equiv.) was added. The mixture was refluxed with stirring for 15 min. After this time, the solution of an appropriate N1-bromoalkyl-3-benzyl-5,5-dimethylhydantoin derivatives (3–8, 4.8 mmol, 1.2 equiv) in acetone (10 mL) was added and the reaction mixture was refluxed for 4–10 h. After the completion of the reaction, the inorganic precipitate was filtered off. The filtrate was concentrated in vacuo, and the residue was dissolved in DCM (20 mL) and washed three times with 1 % HCl (3 \times 20 mL). The collected organic fraction was dried with anhydrous Na_2SO_4 and concentrated. The final product was further transformed into hydrochloride salt via saturation with hydrochloride gas. The suspension was left for 24 h in the refrigerator (2–8 $^\circ\text{C}$) to complete precipitation, then filtered off, followed by drying the precipitate at room temperature.

3-(2,4-Dichlorobenzyl)-1-(5-(4-(2-methoxyphenyl)piperazin-1-yl)pentyl)-5,5-dimethylimidazolidine-2,4-dione (9). White solid. Yield 24 %, mp = 221–222 $^\circ\text{C}$, purity 99.04 %. ^1H NMR (300 MHz, $\text{DMSO}-d_6$) δ 10.40 (s, 1H), 7.65 (s, 1H), 7.43 (d, $J=7.8$ Hz, 1H), 7.17 (d, $J=8.0$ Hz, 1H), 7.00 (d, $J=9.8$ Hz, 2H), 6.91 (d, $J=6.9$ Hz, 2H), 4.61 (s, 2H), 3.78 (s, 3H), 3.56–3.42 (m, 4H), 3.31–3.23 (m, 2H), 3.11 (s, 4H), 3.05–2.96 (m, 2H), 1.75 (s, 2H), 1.65–1.55 (m, 2H), 1.38 (s, 6H), 1.22 (s, 2H). ^{13}C NMR (126 MHz, $\text{DMSO}-d_6$) δ 176.10, 154.33, 151.84, 139.01, 132.84, 132.72, 129.88, 128.95, 127.71, 123.80, 120.88, 118.41, 112.02, 61.74, 55.43, 55.30, 50.88, 46.89, 28.61, 23.54, 22.62, 22.59. MS (ESI) m/z calculated for $[\text{C}_{28}\text{H}_{37}\text{Cl}_2\text{N}_4\text{O}_3]^+$ $[\text{M}+\text{H}]^+$ 547.22, found 547.17. HR-MS (ESI-QTOF) calcd for $[\text{C}_{28}\text{H}_{37}\text{Cl}_2\text{N}_4\text{O}_3]^+$ $[\text{M}+\text{H}]^+$: 547.2238, found: 547.2277.

2-(4-(5-(3-(2,4-Dichlorobenzyl)-5,5-dimethyl-2,4-dioximidazolidin-1-yl)pentyl)piperazin-1-yl)benzonitrile (10). White solid. Yield 51 %, mp = 113–114 $^\circ\text{C}$, purity 100 %. ^1H NMR (300 MHz, $\text{DMSO}-d_6$) δ 10.21 (s, 1H), 7.76 (d, $J=7.6$ Hz, 1H), 7.68–7.60 (m, 2H), 7.42 (dd, $J=8.4$, 2.2 Hz, 1H), 7.26–7.20 (m, 1H), 7.17 (d, $J=8.4$ Hz, 2H), 4.61 (s, 2H), 3.61 (s, 4H), 3.26 (t, $J=7.6$ Hz, 4H), 3.21–3.12 (m, 4H), 1.80–1.69 (m, 2H), 1.66–1.55 (m, 2H), 1.38 (s, 6H), 1.35–1.26 (m, 2H). ^{13}C NMR (126 MHz, $\text{DMSO}-d_6$) δ 176.07, 154.32, 153.78, 134.57, 134.32, 132.83, 132.73, 132.72, 132.72, 132.71, 129.89, 128.94, 127.68, 123.12, 119.44, 117.94, 105.21, 61.73, 61.72, 61.71, 55.30, 50.93, 50.89, 48.09, 28.61, 23.49, 22.69, 22.61. MS (ESI) m/z calculated for $[\text{C}_{28}\text{H}_{34}\text{Cl}_2\text{N}_5\text{O}_2]^+$ $[\text{M}+\text{H}]^+$ 542.21, found 542.12. HR-MS (ESI-QTOF) calcd for $[\text{C}_{28}\text{H}_{34}\text{Cl}_2\text{N}_5\text{O}_2]^+$ $[\text{M}+\text{H}]^+$: 542.2085, found: 542.2108.

3-(2,4-Dichlorobenzyl)-1-(4-(4-(2-methoxyphenyl)piperazin-1-yl)butyl)-5,5-dimethylimidazolidine-2,4-dione (11). White solid. Yield 6.8 %, mp = 117–118 $^\circ\text{C}$, purity 95.83 %. ^1H NMR (300 MHz, $\text{DMSO}-d_6$) δ 10.14 (s, 1H), 7.65 (d, $J=2.1$ Hz, 1H), 7.43 (dd, $J=8.4$, 2.2 Hz, 1H), 7.19 (d, $J=8.4$ Hz, 1H), 7.06–6.97 (m, 2H), 6.97–6.87 (m, 2H), 4.62 (s, 2H), 3.78 (s, 3H), 3.50 (s, 4H), 3.36–3.28 (m, 4H), 3.16–3.07 (m, 2H), 2.98 (t, $J=11.9$ Hz, 2H), 1.79–1.69 (m, 2H), 1.66–1.56 (m, $J=6.3$ Hz, 2H), 1.39 (s, 6H). ^{13}C NMR (126 MHz, $\text{DMSO}-d_6$) δ 176.04, 154.45, 151.83, 139.39, 132.80, 132.69, 132.67, 129.84, 128.92, 127.74, 123.51, 120.85, 118.25, 111.91, 61.77, 55.39, 51.13, 46.88, 26.30, 22.60, 20.54. MS (ESI) m/z calculated for $[\text{C}_{27}\text{H}_{35}\text{Cl}_2\text{N}_4\text{O}_3]^+$ $[\text{M}+\text{H}]^+$ 533.21,

found 533.15. HR-MS (ESI-QTOF) calcd for $[\text{C}_{27}\text{H}_{35}\text{Cl}_2\text{N}_4\text{O}_3]^+$ $[\text{M}+\text{H}]^+$: 533.2081, found: 533.2115.

3-(2,4-Dichlorobenzyl)-1-(4-(4-(3,4-dichlorophenyl)piperazin-1-yl)butyl)-5,5-dimethylimidazolidine-2,4-dione (12). White solid. Yield 36 %, mp = 173–174 $^\circ\text{C}$, purity 97.86 %. ^1H NMR (300 MHz, $\text{DMSO}-d_6$) δ 9.98 (s, 1H), 7.65 (d, $J=2.1$ Hz, 1H), 7.48–7.40 (m, 2H), 7.24 (s, 1H), 7.18 (d, $J=8.3$ Hz, 1H), 7.02 (s, 1H), 4.61 (s, 2H), 3.89 (s, 2H), 3.51 (d, $J=6.0$ Hz, 2H), 3.20–3.02 (m, 2H), 3.09 (s, 4H), 1.77–1.64 (m, 2H), 1.64–1.52 (m, 2H), 1.38 (s, 6H), 1.22 (s, 2H). ^{13}C NMR (126 MHz, $\text{DMSO}-d_6$) δ 176.03, 154.42, 149.32, 132.79, 132.67, 132.65, 131.68, 131.67, 130.67, 129.81, 128.91, 127.74, 120.83, 117.01, 115.86, 61.75, 54.91, 50.15, 44.71, 38.55, 26.31, 22.59, 20.47. MS (ESI) m/z calculated for $[\text{C}_{26}\text{H}_{31}\text{Cl}_4\text{N}_4\text{O}_2]^+$ $[\text{M}+\text{H}]^+$ 571.12, found 571.03. HR-MS (ESI-QTOF) calcd for $[\text{C}_{26}\text{H}_{31}\text{Cl}_4\text{N}_4\text{O}_2]^+$ $[\text{M}+\text{H}]^+$: 573.1167, found: 573.1263.

3-(2,4-Dichlorobenzyl)-1-(3-(4-(3,4-dichlorophenyl)piperazin-1-yl)propyl)-5,5-dimethylimidazolidine-2,4-dione (13). White solid. Yield 86 %, mp = 217–218 $^\circ\text{C}$, purity 97.02 %. ^1H NMR (300 MHz, $\text{DMSO}-d_6$) δ 10.66 (s, 1H), 7.64 (d, $J=2.1$ Hz, 1H), 7.47–7.39 (m, 2H), 7.24 (d, $J=2.7$ Hz, 1H), 7.20 (d, $J=8.4$ Hz, 1H), 6.99 (dd, $J=9.0$, 2.9 Hz, 1H), 4.62 (s, 2H), 3.89 (d, $J=12.3$ Hz, 2H), 3.52 (d, $J=11.2$ Hz, 2H), 3.39 (t, $J=7.0$ Hz, 2H), 3.23–3.16 (m, 2H), 3.15–3.01 (m, 4H), 2.09–1.96 (m, 2H), 1.40 (s, 6H). ^{13}C NMR (126 MHz, $\text{DMSO}-d_6$) δ 176.03, 154.61, 149.29, 132.83, 132.70, 132.59, 131.68, 130.67, 129.88, 128.92, 127.67, 120.79, 117.00, 115.83, 61.84, 53.10, 50.23, 44.71, 36.57, 23.66, 22.55. MS (ESI) m/z calculated for $[\text{C}_{25}\text{H}_{29}\text{Cl}_4\text{N}_4\text{O}_3]^+$ $[\text{M}+\text{H}]^+$ 557.10, found 557.01. HR-MS (ESI-QTOF) calcd for $[\text{C}_{25}\text{H}_{29}\text{Cl}_4\text{N}_4\text{O}_3]^+$ $[\text{M}+\text{H}]^+$: 559.1010, found: 559.1036.

3-(4-Chlorobenzyl)-1-(6-(4-(2-methoxyphenyl)piperazin-1-yl)hexyl)-5,5-dimethylimidazolidine-2,4-dione (14). White solid. Yield 13 %, mp = 208–209 $^\circ\text{C}$, purity 100 %. ^1H NMR (300 MHz, $\text{DMSO}-d_6$) δ 10.91 (s, 1H), 7.39 (d, $J=8.5$ Hz, 2H), 7.23 (d, $J=8.5$ Hz, 2H), 7.06–6.96 (m, 2H), 6.96–6.85 (m, 2H), 4.53 (s, 2H), 3.78 (s, 3H), 3.48 (dd, $J=13.6$, 9.3 Hz, 4H), 3.28–3.19 (m, 2H), 3.08 (q, $J=9.5$ Hz, 6H), 1.80–1.65 (m, 2H), 1.62–1.50 (m, 2H), 1.33 (s, 6H), 1.32–1.30 (m, 2H), 1.30–1.20 (m, 2H). ^{13}C NMR (126 MHz, $\text{DMSO}-d_6$) δ 176.18, 154.47, 151.84, 138.97, 135.78, 132.07, 129.14, 128.65, 123.82, 120.89, 118.43, 112.03, 61.59, 55.44, 55.40, 50.87, 46.91, 40.70, 28.95, 25.91, 25.83, 22.91, 22.62. MS (ESI) m/z calculated for $[\text{C}_{29}\text{H}_{40}\text{ClN}_4\text{O}_3]^+$ $[\text{M}+\text{H}]^+$ 527.28, found 527.53. HR-MS (ESI-QTOF) calcd for $[\text{C}_{29}\text{H}_{40}\text{ClN}_4\text{O}_3]^+$ $[\text{M}+\text{H}]^+$: 527.2784, found: 527.2809.

3-(4-Chlorobenzyl)-5,5-dimethyl-1-(5-(4-phenylpiperazin-1-yl)pentyl)imidazolidine-2,4-dione (15). White solid. Yield 64 %, mp = 199–200 $^\circ\text{C}$, purity 97.49 %. ^1H NMR (300 MHz, $\text{DMSO}-d_6$) δ 10.63 (s, 1H), 7.40 (d, $J=8.5$ Hz, 2H), 7.25 (dd, $J=8.5$, 6.5 Hz, 4H), 6.99 (d, $J=7.9$ Hz, 2H), 6.85 (t, $J=7.2$ Hz, 1H), 4.54 (s, 2H), 3.79 (d, $J=8.9$ Hz, 2H), 3.53 (d, $J=5.3$ Hz, 2H), 3.29–3.22 (m, 2H), 3.18–3.01 (m, 6H), 1.83–1.67 (m, 2H), 1.65–1.52 (m, 2H), 1.34 (s, 6H), 1.33–1.26 (m, 2H). ^{13}C NMR (126 MHz, $\text{DMSO}-d_6$) δ 176.15, 154.50, 149.65, 135.75, 132.06, 132.06, 129.14, 129.13, 128.66, 128.63, 119.95, 115.94, 115.90, 61.59, 55.16, 50.49, 45.32, 40.68, 28.61, 23.52, 22.58. MS (ESI) m/z calculated for $[\text{C}_{27}\text{H}_{36}\text{ClN}_4\text{O}_2]^+$ $[\text{M}+\text{H}]^+$ 483.25, found 483.23. HR-MS (ESI-QTOF) calcd for $[\text{C}_{27}\text{H}_{36}\text{ClN}_4\text{O}_2]^+$ $[\text{M}+\text{H}]^+$: 483.2522, found: 483.2603.

3-(4-Chlorobenzyl)-1-(5-(4-(2-methoxyphenyl)piperazin-1-yl)pentyl)-5,5-dimethylimidazolidine-2,4-dione (16). White solid. Yield 22 %, mp = 228–229 $^\circ\text{C}$, purity 100 %. ^1H NMR (300 MHz, $\text{DMSO}-d_6$) δ 10.96 (s, 1H), 7.40 (d, $J=8.5$ Hz, 2H), 7.24 (d, $J=8.5$ Hz, 2H), 7.06–6.97 (m, 2H), 6.97–6.88 (m, 2H), 4.54 (s, 2H), 3.78 (s, 3H), 3.48 (dd, $J=13.5$, 9.1 Hz, 4H), 3.31–3.21 (m, 2H), 3.13 (dd, $J=20.5$, 11.3 Hz, 6H), 1.83–1.68 (m, 2H), 1.66–1.52 (m, 2H), 1.35 (s, 6H), 1.33–1.25 (m, 2H). ^{13}C NMR (126 MHz, $\text{DMSO}-d_6$) δ 176.18, 154.53, 151.85, 135.77, 132.08, 132.07, 129.14, 128.65, 123.83, 120.88, 118.43, 112.03, 61.62, 55.44, 50.85, 46.90, 40.71, 28.61, 23.55, 22.60, 22.58. MS (ESI) m/z calculated for $[\text{C}_{28}\text{H}_{38}\text{ClN}_4\text{O}_3]^+$ $[\text{M}+\text{H}]^+$ 513.26, found 513.57. HR-MS (ESI-QTOF) calcd for $[\text{C}_{28}\text{H}_{38}\text{ClN}_4\text{O}_3]^+$ $[\text{M}+\text{H}]^+$: 513.2627, found: 513.2675.

3-(2,4-Dichlorobenzyl)-5,5-dimethyl-1-(6-(4-phenylpiperazin-1-yl)hexyl)imidazolidine-2,4-dione (17). White solid. Yield 64 %, mp =

203–205 °C, purity 100 %. ^1H NMR (300 MHz, DMSO- d_6) δ 11.06 (s, 1H), 7.64 (d, $J=2.1$ Hz, 1H), 7.42 (dd, $J=8.3$, 2.2 Hz, 1H), 7.25 (dd, $J=8.7$, 7.3 Hz, 2H), 7.16 (d, $J=8.4$ Hz, 1H), 6.99 (d, $J=7.9$ Hz, 2H), 6.85 (t, $J=7.3$ Hz, 1H), 4.61 (s, 2H), 3.77 (d, $J=11.9$ Hz, 2H), 3.52 (d, $J=11.4$ Hz, 2H), 3.29–3.21 (m, 2H), 3.19–2.97 (m, 6H), 1.80–1.66 (m, 2H), 1.58 (p, $J=8.0$ Hz, 2H), 1.37 (s, 6H), 1.32 (s, 4H). ^{13}C NMR (126 MHz, DMSO- d_6) δ 176.10, 154.28, 149.40, 132.83, 132.74, 132.73, 129.88, 129.20, 128.95, 127.71, 120.31, 116.14, 61.70, 55.26, 50.39, 45.48, 28.95, 25.90, 25.85, 22.90, 22.65. MS (ESI) m/z calculated for $[\text{C}_{28}\text{H}_{37}\text{Cl}_2\text{N}_4\text{O}_2]^+ [\text{M}+\text{H}]^+$ 531.23, found 531.52. HR-MS (ESI-QTOF) calcd for $[\text{C}_{28}\text{H}_{37}\text{Cl}_2\text{N}_4\text{O}_2]^+ [\text{M}+\text{H}]^+$: 531.2289, found: 531.2369.

3-(2,4-Dichlorobenzyl)-1-(6-(4-(3,4-dimethylphenyl)piperazin-1-yl)hexyl)-5,5-dimethylimidazolidine-2,4-dione (18). White solid. Yield 38 %, mp = 209–211 °C, purity 97.88 %, ^1H NMR (300 MHz, DMSO- d_6) δ 11.01 (s, 1H), 7.64 (d, $J=2.1$ Hz, 1H), 7.42 (dd, $J=8.4$, 2.2 Hz, 1H), 7.16 (d, $J=8.4$ Hz, 1H), 7.00 (d, $J=8.3$ Hz, 1H), 6.81 (d, $J=2.3$ Hz, 1H), 6.71 (dd, $J=8.3$, 2.5 Hz, 1H), 4.60 (s, 2H), 3.69 (d, $J=10.8$ Hz, 2H), 3.50 (d, $J=9.2$ Hz, 2H), 3.30–3.21 (m, 2H), 3.11 (dd, $J=23.5$, 12.0 Hz, 6H), 2.17 (s, 3H), 2.11 (s, 3H), 1.81–1.65 (m, 2H), 1.65–1.50 (m, 2H), 1.37 (s, 6H), 1.32 (s, 4H). ^{13}C NMR (126 MHz, DMSO- d_6) δ 176.09, 154.28, 136.96, 132.83, 132.74, 132.73, 132.72, 130.15, 129.88, 128.95, 127.71, 118.17, 114.19, 61.70, 61.68, 55.25, 50.21, 46.37, 28.95, 25.90, 25.83, 22.91, 22.64, 19.81, 18.54. MS (ESI) m/z calculated for $[\text{C}_{30}\text{H}_{41}\text{Cl}_2\text{N}_4\text{O}_2]^+ [\text{M}+\text{H}]^+$ 559.26, found 559.51. HR-MS (ESI-QTOF) calcd for $[\text{C}_{30}\text{H}_{41}\text{Cl}_2\text{N}_4\text{O}_2]^+ [\text{M}+\text{H}]^+$: 559.2602, found: 559.2700.

4.1.4. Procedure for the synthesis of 3-(2,4-dichlorobenzyl)-1-(3-(4-(2,3-dichlorophenyl)piperazin-1-yl)-2-hydroxypropyl)-5,5-dimethylimidazolidine-2,4-dione (20)

Equal amounts of 1-(2,3-dichlorophenyl)piperazine (3.0 mmol) and 3-(2,4-dichlorobenzyl)-1-(2-methylepoxypropane)-5,5-dimethylhydantoin (3.0 mmol) were dissolved in acetone (20 mL). The solution was then concentrated in vacuo to remove the solvent, and the homogeneous residue was subjected to the reaction in a microwave oven (300–450 W) for 4 min. The final product was converted to the relative hydrochloride salt and crystallised from diethyl ether.

White solid. Yield 63 %, mp = 224–225 °C, purity 97.96 %. ^1H NMR (300 MHz, DMSO- d_6) δ 10.57 (s, 1H), 7.65 (d, $J=2.1$ Hz, 1H), 7.42 (dd, $J=8.4$, 2.1 Hz, 1H), 7.38–7.33 (m, 2H), 7.25 (d, $J=8.4$ Hz, 1H), 7.20 (dd, $J=6.7$, 2.9 Hz, 1H), 5.93 (s, 1H), 4.63 (s, 2H), 4.36 (s, 1H), 3.63 (dd, $J=37.7$, 9.4 Hz, 2H), 3.48–3.35 (m, 4H), 3.25 (d, $J=8.5$ Hz, 4H), 3.14 (dd, $J=20.1$, 10.6 Hz, 2H), 1.43 (d, $J=6.2$ Hz, 6H). ^{13}C NMR (126 MHz, DMSO- d_6) δ 176.13, 155.04, 149.58, 132.81, 132.76, 132.68, 132.55, 129.90, 128.88, 128.68, 127.68, 126.06, 126.05, 125.27, 119.79, 63.79, 61.97, 58.95, 52.64, 51.26, 47.64, 47.54, 43.67, 22.76, 22.63. MS (ESI) m/z calculated for $[\text{C}_{25}\text{H}_{29}\text{Cl}_4\text{N}_4\text{O}_3]^+ [\text{M}+\text{H}]^+$ 573.10, found 573.09. HR-MS (ESI-QTOF) calcd for $[\text{C}_{25}\text{H}_{29}\text{Cl}_4\text{N}_4\text{O}_3]^+ [\text{M}+\text{H}]^+$: 575.0959, found: 575.1022.

4.1.5. General procedure for the synthesis of hydantoin of final compounds within group B (30–32)

The appropriate derivative of phenylpiperazine (2 mmol) was dissolved in 15 mL of isopropanol with the addition of K_2CO_3 (4 mmol, 2 equiv.). The mixture was stirred for approximately 10 min, then 5-(4-fluorophenyl)-5-methyl-3-(oxiran-2-ylmethyl)imidazolidine-2,4-dione (2.4 mmol, 1.2 equiv.) was added. The reaction was refluxed for 4 h and then left overnight at room temperature. Next, after the removal of isopropanol in vacuo, the residue was suspended in 20 mL of distilled water and extracted with DCM (4x20 mL). The organic layer was dried over anhydrous Na_2SO_4 and evaporated. The product was purified by flash chromatography with DCM and MeOH (Method A) or 2 % ammonium solution in MeOH (Method B).

5-(4-Fluorophenyl)-3-(2-hydroxy-3-(4-(2-isobutoxyphenyl)piperazin-1-yl)propyl)-5-methylimidazolidine-2,4-dione (30). Method A. White solid. Yield 27.4 %, mp = 56–58 °C, purity 100 %. ^1H NMR (500 MHz, DMSO- d_6) δ 8.88 (s, 1H), 7.52 (ddd, $J=9.1$, 5.3, 3.8 Hz, 2H), 7.20 (td,

$J=8.9$, 5.2 Hz, 2H), 6.87 (d, $J=2.1$ Hz, 2H), 6.82 (ddd, $J=5.5$, 2.8, 1.5 Hz, 2H), 4.84 (dd, $J=11.0$, 5.6 Hz, 1H), 3.90 (dt, $J=8.4$, 6.4 Hz, 1H), 3.71 (d, $J=6.2$ Hz, 2H), 3.42–3.35 (m, 2H), 2.91 (s, 4H), 2.46 (s, 4H), 2.28 (dd, $J=12.0$, 6.2 Hz, 2H), 2.06–1.97 (m, 1H), 1.66 (s, 2H), 0.99 (d, $J=6.7$ Hz, 6H). ^{13}C NMR (126 MHz, DMSO- d_6) δ 175.91, 163.23, 161.28, 156.37, 151.85, 141.79, 136.59, 128.25, 122.71, 121.20, 118.27, 115.74, 113.00, 74.27, 65.07, 63.17, 62.75, 55.44, 54.26, 50.52, 43.64, 28.60, 25.76, 19.79. MS (ESI) m/z calculated for $[\text{C}_{27}\text{H}_{36}\text{FN}_4\text{O}_4]^+ [\text{M}+\text{H}]^+$ 499.27, found 449.32. HR-MS (ESI-QTOF) calcd for $[\text{C}_{27}\text{H}_{36}\text{FN}_4\text{O}_4]^+ [\text{M}+\text{H}]^+$: 499.2716, found: 499.2768.

5-(4-Fluorophenyl)-3-(2-hydroxy-3-(4-(2-(naphthalen-1-ylmethoxy)phenyl)piperazin-1-yl)propyl)-5-methylimidazolidine-2,4-dione (31). Method A. Yellowish solid. Yield 51.1 %, mp = 94–95 °C, purity 100 %. ^1H NMR (500 MHz, DMSO- d_6) δ 8.87 (s, 1H), 8.18 (d, $J=9.0$ Hz, 1H), 7.96 (d, $J=9.4$ Hz, 1H), 7.91 (d, $J=8.2$ Hz, 1H), 7.71 (d, $J=6.9$ Hz, 1H), 7.60–7.54 (m, 2H), 7.54–7.47 (m, 3H), 7.23–7.17 (m, 3H), 6.98–6.93 (m, 1H), 6.92–6.86 (m, 2H), 5.55 (s, 2H), 4.80 (dd, $J=10.2$, 5.6 Hz, 1H), 3.92–3.81 (m, 1H), 3.46–3.33 (m, 2H), 2.91 (s, 4H), 2.40 (d, $J=25.1$ Hz, 4H), 2.27–2.19 (m, 2H), 1.65 (s, 3H). NMR (126 MHz, DMSO- d_6) δ 207.05, 175.90, 163.23, 161.28, 156.36, 151.60, 142.41, 136.60, 133.74, 133.52, 131.34, 128.94, 128.26, 126.77, 126.47, 126.21, 125.89, 124.55, 122.87, 121.97, 118.72, 115.75, 114.61, 68.60, 65.03, 63.10, 62.74, 54.06, 50.68, 43.63, 31.23, 25.81. MS (ESI) m/z calculated for $[\text{C}_{34}\text{H}_{36}\text{FN}_4\text{O}_4]^+ [\text{M}+\text{H}]^+$ 583.27, found 583.33. HR-MS (ESI-QTOF) calcd for $[\text{C}_{34}\text{H}_{36}\text{FN}_4\text{O}_4]^+ [\text{M}+\text{H}]^+$: 583.2716, found: 583.2758.

3-(3-(4-(2-(3-(Dimethylamino)propoxy)phenyl)piperazin-1-yl)-2-hydroxypropyl)-5-(4-fluorophenyl)-5-methylimidazolidine-2,4-dione (32). Method B. White solid. Yield 11.8 %, mp = 70–72 °C, purity 100 %. ^1H NMR (500 MHz, DMSO- d_6) δ 8.88 (s, 1H), 7.52 (ddd, $J=9.3$, 5.3, 4.2 Hz, 2H), 7.21 (td, $J=8.9$, 5.4 Hz, 2H), 6.88 (dd, $J=6.0$, 1.9 Hz, 2H), 6.85–6.79 (m, 2H), 4.84 (dd, $J=11.3$, 5.6 Hz, 1H), 3.94 (t, $J=6.1$ Hz, 2H), 3.93–3.85 (m, 1H), 3.44–3.36 (m, 2H), 2.90 (s, 4H), 2.46 (s, 4H), 2.39 (t, $J=7.2$ Hz, 2H), 2.28 (dd, $J=10.6$, 6.4 Hz, 2H), 2.14 (d, $J=0.5$ Hz, 6H), 1.87–1.79 (m, 2H), 1.66 (s, 3H). ^{13}C NMR (126 MHz, DMSO- d_6) δ 175.90, 163.22, 161.28, 156.37, 151.78, 141.87, 136.59, 128.25, 122.73, 121.33, 118.33, 115.75, 113.29, 66.20, 65.07, 63.18, 62.74, 56.44, 54.22, 50.48, 45.71, 43.66, 27.54, 25.80. MS (ESI) m/z calculated for $[\text{C}_{28}\text{H}_{39}\text{FN}_5\text{O}_4]^+ [\text{M}+\text{H}]^+$ 528.30, found 528.30. HR-MS (ESI-QTOF) calcd for $[\text{C}_{28}\text{H}_{39}\text{FN}_5\text{O}_4]^+ [\text{M}+\text{H}]^+$: 528.2981, found: 528.3044.

4.2. In silico studies

4.2.1. Docking studies

The compounds were prepared for docking (generation of three-dimensional conformations and protonation states at pH=7.4) in Lig-Prep (Schrödinger Suite 2023-2) [60]. The following proteins were used: inactive-state 5-HT₇R, 5-HT₆R, and 5-HT_{1A}R homology models deposited in the GPCRdb [29] (due to the predicted antagonistic properties of the synthesised compounds despite the available crystal/cryo-EM structures of these proteins in the active conformation), the crystal structure of 5-HT_{2A}R (PDBID: 7WC8 [61]), and D₂R (PDBID: 6CM4 [62]), the cryo-EM structure of the hERG potassium channel (PDBID: 7CN1 [63]), and crystal structure of the human serum albumin (PDBID: 1AO6 [64]). The proteins were prepared for docking using the Protein Preparation Wizard [65]. The grid was centred on the aspartic acid from the third transmembrane helix (D3x32 according to the GPCRdb numbering). The docking was carried out in Glide [66] with extra precision. The docking pose was returned based on the following criteria: a pose was kept if the sum of its Coulomb and van der Waals interaction energies (expressed as the Glide coulomb-vdW score) is lower than 0.0 kcal/mol.

4.2.2. Computational studies for ADMET

Online platforms characterised in Table 4 were used in the study. In addition, the QikProp [52] from the Schrodinger Suite 2023 was applied

(prior to the application of this tool, the 3-dimensional compound conformations and their respective protonation states in the pH=7.4 were generated with the use of LigPrep [60].

4.3. In vitro experiments

4.3.1. Affinity experiments

HEK293 cells stably expressing the human 5-HT_{1A}, 5-HT₆, 5-HT_{7B}, and D₂ receptors and CHO-K1 cells expressing 5-HT_{2A}R (prepared with the use of the Lipofectamine 2000) were maintained at 37 °C in a humidified atmosphere with 5 % CO₂ and grown in Dulbecco's Modified Eagle Medium containing 10 % dialysed foetal bovine serum and 500 µg/mL G418 sulphate. For membrane preparation, the cells were sub-cultured in 150 cm² flasks, grown to 90 % confluence, washed twice with phosphate-buffered saline (PBS) prewarmed to 37 °C and pelleted by centrifugation (200g) in PBS containing 0.1 mM EDTA and 1 mM dithiothreitol. Prior to membrane preparation, the pellets were stored at –80 °C.

The cell pellets were thawed and homogenised in 10 volumes of assay buffer using an Ultra Turrax tissue homogeniser and centrifuged twice at 35,000 g for 20 min at 4 °C, with a 15 min incubation at 37 °C between spins. The composition of the assay buffer is as follows:

5-HT_{1A} – 50 mM Tris–HCl, 0.1 mM EDTA, 4 mM MgCl₂, 10 µM pargyline and 0.1 % ascorbate; 5-HT_{2A} – 50 mM Tris–HCl, 0.1 mM EDTA, 4 mM MgCl₂, and 0.1 % ascorbate; 5-HT₆ – 50 mM Tris–HCl, 0.5 mM EDTA and 4 mM MgCl₂; 5-HT_{7B} – 50 mM Tris–HCl, 4 mM MgCl₂, 10 µM pargyline and 0.1 % ascorbate, D₂ – 50 mM Tris–HCl, 1 mM EDTA, 4 mM MgCl₂, 120 mM NaCl, 5 mM KCl, 1.5 mM CaCl₂ and 0.1 % ascorbate.

The assays were incubated in a total volume of 200 µl on 96-well microtiter plates for 1 h (37 °C, except for 5-HT_{1A} and 5-HT_{2A}, which were incubated at room temperature). The process of equilibration was terminated with rapid filtration through Unifilter GF/B plates (96-well cell harvester, PerkinElmer), and the radioactivity retained on the filters was quantified on a Microbeta plate reader (PerkinElmer). For displacement studies, the assay samples contained the following as radioligands: 2.5 nM [3H]-8-OHDPAT (187 Ci/mmol; 6919 GBq/mmol) – 5-HT_{1A}; 1 nM [3H]-ketanserin (53.4 Ci/mmol; 1975.8 GBq/mmol) – 5-HT_{2A}; 2 nM [3H]-LSD (85 Ci/mmol; 3145 GBq/mmol) – 5-HT₆; 0.8 nM [3H]-5-CT (39.2 Ci/mmol; 1450.4 GBq/mmol) – 5-HT_{7B}; [3H]-raclopride (74.4 Ci/mmol) – D₂R.

Nonspecific binding was defined with 10 µM of 5-HT (5-HT_{1A}, 5-HT_{7B}), 10 µM of chlorpromazine (5-HT_{2A}R), 10 µM of methiothepine (5-HT₆R), or 1 mM of (+)-butaclamol (D₂R).

Each compound was tested at 7 concentrations (10^{–10}–10^{–4} M). The inhibition constants (K_i) were calculated from the Cheng-Prusoff equation [67].

4.3.2. Cardiotoxicity

Compound cardiotoxicity was assessed as affinity to the human ether-a-go-go-related gene (hERG), a prominent component of the potassium channel, with the use of the Invitrogen's Predictor™ hERG Fluorescence Polarization Assay, including Predictor™ Tracer Red, Predictor™ hERG Membrane, Predictor™ hERG FB assay buffer, and E-4031 (reference substrate, 3 mM H₂O solution). Compound dilutions in Predictor™ hERG FB assay buffer were prepared in 5 concentrations (ranging from 340 ng/mL to 440 µg/mL). Each well (384-well black microplates were used to provide blockage of the scattered light, prevent the signal leaking from neighbouring wells and to avoid change in polarisation as a result of reflection) contained 5 µL of the compound solution, 10 µL of hERG Membrane solution and 5 µL of 4 nM Tracer solution. At first, short incubation at room temperature (10 min), the assay plate was covered with a lid and incubated at room temperature for 4 h (it was reassured that the plate was kept away from light). VICTOR Nivo Multimode Microplate Reader was used to gather data and determine the polarisation (mP) scores.

4.3.3. Hepatotoxicity

Hepatotoxicity was examined using the HepaRG – immortalised hepatic cell line retaining many characteristics of primary human hepatocytes (morphology, expression of key metabolic enzymes, expression of nuclear receptors, and drug transporters). The compounds were examined in a dose-dependent toxicity assay utilising a HepaRG cell line incubated in the presence of the studied substance for 72 h. The incubation was followed by the viability measurements (quantification of the present ATP, which is proportional to the number and viability of cells). The HepaRG cells were seeded onto 384-well plates directly from thawed stocks. William's Medium supplemented with Hepatocyte Maintenance Supplement Pack and Glutamax (without fetal bovine serum to avoid potential binding of compounds to its proteins) was used for cell sustaining. Penicillin and streptomycin additives were used in the final concentrations recommended by producers.

The culture medium was incubated in a water bath to reach 37 °C; then the medium flask was drained with a paper towel, decontaminated with 70 % ethanol and placed under a sterile, laminar flow cabinet; 10 mL of the medium was dispensed into a conical bottom 50 mL tube. A vial containing circa 10 million HepaRG cells was removed from liquid nitrogen and quickly warmed up in a hot water bath. Then, the cells were poured into a prepared 50 mL tube. The conical bottom 50 mL tube with cell suspension was centrifugated at 200 × g at room temperature for 5 min. Then, the supernatant was removed, and the cell supernatant was resuspended in 1 mL of Culture Medium. The cells were counted using Trypan Blue to mark the dead cells and an automated cell counter. If the viability exceeded 95 % cells, they were diluted to a concentration of 111 000 cells/mL, and the suspension was distributed into 384 well plates. Seeding density was around 5 000 cells per well, and the volume equaled to 45 µL. The cells were centrifugated at 70 × g for 3 min to ensure the descent of cells to the bottom of the plate. The plate was incubated for the night at 37 °C, 5 % CO₂. The next day, the compound solutions were added (7 concentrations for each compound were prepared).

Stock solutions, 20 mM in DMSO, were used to prepare the intermediate dilution series. Each dilution step was a 10-fold decrease. DMSO was adjusted in controls and lower concentrations to match 0.25 % in the final sample. The range of final concentrations of tested compounds was from 50 pM to 50 µM.

The plates were incubated at 37 °C, 5 % CO₂, for 72 h. Then, plates were placed at room temperature to equilibrate. 50 µL of reconstituted CellTiter-Glo® Luminescent Cell Viability Assay solution was added to each well. The plates were shortly stirred and centrifugated if necessary, to ensure the lysis. The luminescence corresponding to the level of ATP and, therefore, cell number and viability was read with Tecan SPARK.

4.3.4. Membrane permeability

The ability of compounds to cross biological barriers was tested using cell lines derived from human colon Caco-2 (passive permeability was tested). At first, 3-lane 64 chip Organo plates were prepared: extracellular matrix composed of 4 mg/mL of collagen-I solution (1 M HEPES, 37 g/L NaHCO₃ and collagen-I in 1:1:8 ratio) was dispensed to the central lanes of each chip; then, the plates were placed in an incubator at 37 °C with 5 % of CO₂. Caco-2 cells were thawed according to a standard protocol. 2 µL of inlet cell suspension was dispensed to each well to the right chamber. Then, the inlet and outlets were filled with medium, and the plate was incubated at 37 °C with 5 % CO₂; microtubules were formed after 7 days of incubation. Medium in the right and inlet and outer chamber was replaced with the fresh one, without foetal bovine serum, but spiked with tested compounds at a concentration of 10 µM; the medium also contains inhibitors for active transport, elacridar 5 µM, Ko134 5 µM, valospodar 1 µM, verapamil 10 µM. In parallel, control compounds are tested: atenolol for low permeability, propranolol and pindolol for high permeability. Samples of 20 µL of medium from the right inlets were collected (T₀). The plate was incubated with rocking, ensuring the flow of the liquids. After 24 h of incubation, 20 µL of

medium from the left chambers were collected (T24). Samples from the donor compartment were collected for the recovery investigation as well. Samples were dispensed to deep well extraction plates containing 80 μL of methanol.

Extraction plates were agitated at 700 rpm on a plate vortex for 5 min, then centrifuged for 20 min at $3000 \times g$ at 4°C . The supernatant was collected, diluted with Milli-Q water, and analysed with LC-MS.

4.3.5. Metabolic stability

The assay determined the metabolic stability of tested compounds by incubating their solutions in the presence of primary hepatocytes. The compounds were dissolved in William's medium (previously incubated at 37°C for 30 min. in an assay plate); warfarin (low intrinsic clearance, high stability) and verapamil (high intrinsic clearance, low stability) were tested as a reference. Hepatocytes were thawed, centrifuged, resuspended in William's medium and counted. Cells were diluted to a concentration of 1 million live cells per millilitre. The reaction started with the addition of an equal amount of cell solution. Immediately after mixing the reaction solutions, 20 μL of samples are taken from the reaction plate and dispensed into methanol in the extraction plate. The reaction plate was placed into an incubator on a rocker at 37°C 5 % CO_2 , and the extraction plate was further processed. The procedure of mixing and collecting 20 μL of samples was repeated at time points 15, 30, 60 and 120 min from both reaction samples and controls.

Extraction plates were agitated at 700 rpm on a plate vortex for 5 min, then centrifuged for 20 min at $3000 \times g$ at 4°C . The supernatant was collected, diluted with Milli-Q water, and analysed by LC-MS.

4.3.6. Protein plasma binding

The PPB was assessed via examination of the compound binding to HSA. The binding constant (K_D) and the percentage of fraction bound were determined. The surface plasmon resonance experiments were performed using a Biacore S200 system (Cytiva, Marlborough, MA, USA) equipped with a CM5 sensor chip. The ligand HSA at 40 $\mu\text{g}/\text{mL}$ concentration in 10 mM sodium acetate, pH 4.5, was immobilised using amine-coupling chemistry at a density of 8000 RU on a flow cell with a preceding flow cell left blank for reference. Kinetics analysis was performed in running buffer (140 mM NaCl, 10 mM phosphate buffer, 3 mM KCl, 0.01 % Tween20, 3 % DMSO, pH 7.4), and data were collected at a rate of 10 Hz. Triplicate injections of compounds were injected at concentrations of 15 μM , 5 μM , and 1 μM in single-cycle mode over surfaces simultaneously at a flow rate of 30 $\mu\text{L}/\text{min}$ and a temperature of 20°C , and the surfaces were washed with running buffer for 10 s at 80 $\mu\text{L}/\text{min}$ between each sample injection. Buffer blanks were injected after every sample. DMSO samples containing 2.5–3.75 % DMSO in a running buffer were also injected for a solvent correction plot. The complex was allowed to associate for 60 s and dissociate for 300 s, with no regeneration steps. The data were fit to a Steady State Affinity interaction model using the global data analysis option available within Biacore S200 Evaluation Software 1.1.1 (Cytiva). The conversion from K_D to percentage bound values of tested compounds was performed as presented in Rich et al., 2001 [68].

4.3.7. Neurotoxicity in SH-SY5Y cells

Human neuroblastoma cell line SH-SY5Y (ATCC no. CRL-2266) was used for neurotoxicity evaluation. The cells (8×10^3 cells/100 $\mu\text{L}/\text{well}$) were cultured in transparent 96-well plates (Corning) in DMEM supplemented with 10 % FBS in the presence of DMSO, vehicle control or compounds 30–32 at 1 μM or 10 μM for 72 h. After the incubation time, the cell viability was examined using an MTS-based CellTiter96 Aqueous One Solution Cell Proliferation Assay (Promega, Madison, WI, USA) following the manufacturer's protocol as [69]. The absorbance was measured at 490 nm.

RNA Extraction, Reverse Transcription, and qPCR

RNAs were extracted from SH-SY5Y cells treated with the vehicle (DMSO) or compound 30–32 at 1 μM or 10 μM by ReliaPrep RNA Tissue

Table 10
PCR Primers' Sequences.

Primer name	Primer sequence
hL32 FW	GGAGCGACTGCTACGGAAG
hL32 REV	GATACTGTCCAAAAGGCTGGAA
hNRF-2 FW	AGGTTGCCACATTCCCAA
hNRF-2 REV	ACGTAGCCGAAGAAACCTCA
hHO-1 FW	ACCTTCCCCAACATTGCCAG
hHO-1 REV	CAACTCCTCAAAGAGCTGGATG
hBACE-1 FW	CCCGGGAGACCGACGAA
hBACE-1 REV	CACGAGATGTTGAGCGTCT
hSOD-1 FW	AGGCATGTTGGAGACTTGGG
hSOD-1 REV	TGCTTTTTCATGGACCACCA
hNQO-1 FW	GCTGTTTGGAGGAGTGTTCT
hNQO-1 REV	CTGCCTTCTACTCCGGAAGG
hNFKB FW	GCTTAGGAGGAGAGCCCA
hNFKB REV	CTTCTGCCATTCTGAAGCCG

Miniprep System (Promega) and reverse transcribed with iScriptTM cDNA Synthesis Kit (Bio-Rad Laboratories) accordingly to the respective manufacturer's protocol. cDNAs were amplified by qPCR reaction using GoTaq qPCR Master Mix (Promega), as reported in [70]. Relative amounts obtained with the $2(-\Delta\text{Ct})$ method were normalised with respect to the housekeeping gene L32. The relative PCR primers' sequences are reported in Table 10.

CRediT authorship contribution statement

Patryk Pyka: Writing – original draft, Visualization, Validation, Methodology, Investigation, Formal analysis, Conceptualization. **Sabrina Garbo:** Writing – review & editing, Writing – original draft, Methodology, Investigation, Formal analysis, Data curation. **Aleksandra Murzyn:** Writing – original draft, Visualization, Methodology, Investigation, Conceptualization. **Grzegorz Satała:** Writing – review & editing, Writing – original draft, Visualization, Validation, Methodology, Investigation, Data curation. **Artur Janusz:** Writing – original draft, Validation, Supervision, Methodology, Investigation, Conceptualization. **Michał Górka:** Visualization, Validation, Methodology, Investigation, Conceptualization. **Wojciech Pietrus:** Visualization, Validation, Methodology, Investigation, Conceptualization. **Filip Miś:** Writing – original draft, Visualization, Validation, Methodology, Investigation, Data curation. **Delfina Popiel:** Visualization, Validation, Supervision, Methodology, Investigation. **Maciej Wieczorek:** Supervision, Project administration, Funding acquisition. **Biagio Palmisano:** Writing – original draft, Visualization, Validation, Methodology, Investigation, Data curation. **Alessia Raucci:** Visualization, Validation, Methodology, Investigation. **Andrzej J. Bojarski:** Validation, Supervision. **Clemens Zwergel:** Writing – review & editing, Writing – original draft, Validation, Supervision, Project administration, Investigation, Formal analysis, Conceptualization. **Ewa Szymańska:** Writing – review & editing, Validation, Supervision, Project administration. **Katarzyna Kucwaj-Brysz:** Writing – review & editing, Supervision, Methodology, Investigation. **Cecilia Battistelli:** Writing – review & editing, Validation, Supervision, Project administration, Investigation, Conceptualization. **Jadwiga Handzlik:** Writing – review & editing, Writing – original draft, Visualization, Validation, Supervision, Resources, Project administration, Funding acquisition, Conceptualization. **Sabina Podlewska:** Writing – review & editing, Writing – original draft, Visualization, Validation, Supervision, Software, Resources, Project administration, Investigation, Funding acquisition, Formal analysis, Data curation, Conceptualization.

Declaration of competing interest

The authors declare that they have no known competing financial interests or personal relationships that could have appeared to influence the work reported in this paper.

Acknowledgements

The study was supported by the grant OPUS 2018/31/B/NZ2/00165 (awarded to S. Podlowska) and by the grant PRELUDIUM 2023/49/N/NZ7/02144 (awarded to P. Pyka), financed by the National Science Centre, Poland (<https://www.ncn.gov.pl>). Part of the syntheses (group A) was performed by participants of Student Medicinal Chemistry Club JUCM, Ms. Maria Glomb and Ms. Aleksandra Janik, partly supported by Jagiellonian University Medical College Statutory Project no. N42/DBS/000331. This work was supported by Sapienza SEED PNR 2021 and Sapienza Progetti di Ricerca Medi (RM12218166AEFC72) awarded to C. Battistelli. S. Garbo is supported by Associazione Italiana Ricerca sul Cancro (AIRC). C. Zwergel is thankful for the generous funding from FSE REACT-EU within the program PON "Research and Innovation" 2014–2020, Action IV.6 "Contratti di ricerca su tematiche Green", from Italian Ministry of Health Ricerca Finalizzata GR-2021-12374415 as well as the funding from the KOHR GmbH and the Sapienza Ateneo Project funding scheme. All authors would like to thank Ken Rory and Nick Hinderlaad for their excellent technical assistance, as well as Claus Jacob, Marco Tripodi, Sergio Valente, and Antonello Mai for fruitful discussions and advice.

Appendix A. Supplementary data

Supplementary data to this article can be found online at <https://doi.org/10.1016/j.bioorg.2024.107668>.

References

- C.A. Lipinski, F. Lombardo, B.W. Dominy, P.J. Feeney, Experimental and computational approaches to estimate solubility and permeability in drug discovery and development settings, *Adv. Drug Deliv. Rev.* 46 (2001) 3–26.
- D.F. Veber, S.R. Johnson, H.Y. Cheng, B.R. Smith, K.W. Ward, K.D. Kopple, Molecular properties that influence the oral bioavailability of drug candidates, *J. Med. Chem.* 45 (2002) 2615–2623.
- A.K. Ghose, V.N. Viswanadhan, J.J. Wendoloski, A knowledge-based approach in designing combinatorial or medicinal chemistry libraries for drug discovery. 1. A qualitative and quantitative characterization of known drug databases, *J. Comb. Chem.* 1 (1999) 55–68.
- T.I. Oprea, Property distribution of drug-related chemical databases, *J. Comput. Aided Mol. Des.* 14 (2000) 251–264.
- W.J. Egan, K.M. Merz Jr, J.J. Baldwin, Prediction of drug absorption using multivariate statistics, *J. Med. Chem.* 43 (2000) 3867–3877.
- G.R. Bickerton, G.V. Paolini, J. Besnan, S. Muresan, A.L. Hopkins, Quantifying the chemical beauty of drugs, *Nat. Chem.* 4 (2012) 90–98.
- T.T. Wagner, X. Hou, P.R. Verhoest, A. Villalobos, Moving beyond Rules: The Development of a Central Nervous System Multiparameter Optimization (CNS MPO) Approach To Enable Alignment of Druglike Properties, *ACS Chem. Neurosci.* 1 (2010) 435–449.
- M. Tyagi, F. Begnini, V. Poongavanam, B.C. Doak, J. Kihlberg, Drug Syntheses Beyond the Rule of 5, *Chemistry* 26 (2020) 49–88.
- I.V. Hartung, B.R. Huck, A. Crespo, Rules were made to be broken, *Nat. Rev. Chem.* 7 (2023) 3–4.
- N.E. Daoud, P. Borah, P.K. Deb, K.N. Venugopala, W. Hourani, M. Alzweiri, S. K. Bardaweel, V. Tiwari, ADMET Profiling in Drug Discovery and Development: Perspectives of In Silico, In Vitro and Integrated Approaches, *Curr. Drug Metab.* 22 (2021) 503–522.
- J. Wang, Comprehensive assessment of ADMET risks in drug discovery, *Curr. Pharm. Des.* 15 (2009) 2195–2219.
- T. Kennedy, Managing the drug discovery/development interface, *Drug Disc. Today* 2 (1997) 436–444.
- G.W. Caldwell, Z. Yan, W. Tang, M. Dasgupta, B. Hasting, ADME optimization and toxicity assessment in early- and late-phase drug discovery, *Curr. Top. Med. Chem.* 9 (2009) 965–980.
- A. Yasgar, S.D. Furdas, D.J. Maloney, A. Jadhav, M. Jung, A. Simeonov, High-throughput 1,536-well fluorescence polarization assays for $\alpha(1)$ -acid glycoprotein and human serum albumin binding, *PLoS One* 7 (2012) e45594.
- V. Casadó, V. Casadó-Anguera, What are the current trends in G protein-coupled receptor targeted drug discovery? *Expert Opin. Drug Discov.* 18 (2023) 815–820.
- G.N. Kumar, S. Surapaneni, Role of drug metabolism in drug discovery and development, *Med. Res. Rev.* 21 (2001) 397–411.
- F. Wu, Y. Zhou, L. Li, X. Shen, G. Chen, X. Wang, X. Liang, M. Tan, Z. Huang, Computational Approaches in Preclinical Studies on Drug Discovery and Development, *Front. Chem.* 8 (2020) 726.
- A.S. Hauser, M.M. Attwood, M. Rask-Andersen, H.B. Schiöth, D.E. Gloriam, Trends in GPCR drug discovery: new agents, targets and indications, *Nat. Rev. Drug Discov.* 16 (2017) 829–842.
- D.M. Rosenbaum, S.G. Rasmussen, B.K. Kobilka, The structure and function of G-protein-coupled receptors, *Nature* 459 (2009) 356–363.
- B.C. Heng, D. Aubel, M. Fussenegger, An overview of the diverse roles of G-protein coupled receptors (GPCRs) in the pathophysiology of various human diseases, *Biotechnol. Adv.* 31 (2013) 1676–1694.
- J. Luo, P. Sun, S. Siwko, M. Liu, J. Xiao, The role of GPCRs in bone diseases and dysfunctions, *Bone Res.* 7 (2019) 19.
- A. Egyed, Á.A. Kelemen, M. Vass, A. Visegrády, S.A. Thee, Z. Wang, C. de Graaf, J. Brea, M.I. Loza, R. Leurs, G.M. Keserü, Controlling the selectivity of aminergic GPCR ligands from the extracellular vestibule, *Bioorg. Chem.* 111 (2021) 104832.
- P.B. Hedlund, S. Huitron-Resendiz, S.J. Henriksen, J.G. Sutcliffe, 5-HT₇ receptor inhibition and inactivation induce antidepressant-like behavior and sleep pattern, *Biol. Psychiatry* 58 (2005) 831–837.
- M. Tonini, R. Vicini, E. Cervio, F. De Ponti, R. De Giorgio, G. Barbara, V. Stanghellini, A. Dellabianca, C. Sternini, 5-HT₇ receptors modulate peristalsis and accommodation in the guinea pig ileum, *Gastroenterology* 129 (2005) 1557–1566.
- M. Idzko, E. Panther, C. Stratz, T. Müller, H. Bayer, G. Zissel, T. Dürk, S. Sorichter, F. Di Virgilio, M. Geissler, B. Fiebich, Y. Herouy, P. Elsner, J. Norgauer, D. Ferrari, The serotonergic receptors of human dendritic cells: identification and coupling to cytokine release, *J. Immunol.* 172 (10) (2004) 6011–6060.
- M. Graf, R. Jakus, S. Kantor, G. Levay, G. Bagdy, Selective 5-HT_{1A} and 5-HT₇ antagonists decrease epileptic activity in the WAG/Rij rat model of absence epilepsy, *Neurosci. Lett.* 359 (2004) 45–48.
- Z.S. Gu, Y. Xiao, Q.W. Zhang, J.Q. Li, Synthesis and antidepressant activity of a series of arylalkanol and aralkyl piperazine derivatives targeting SSRI/5-HT_{1A}/5-HT₇, *Bioorg. Med. Chem. Lett.* 27 (2017) 5420–5423.
- M. Azmanova, A. Pitto-Barry, N.P.E. Barry, Schizophrenia: synthetic strategies and recent advances in drug design, *Medchemcomm.* 9 (2018) 759–782.
- G. Pándy-Szekeres, C. Munk, T.M. Tsonkov, S. Mordalski, K. Harpsøe, A.S. Hauser, A.J. Bojarski, D.E. Gloriam, GPCRdb in 2018: adding GPCR structure models and ligands, *Nucleic Acids Res.* 46 (2018) D440–D446.
- J. Handzlik, A.J. Bojarski, G. Satala, M. Kubacka, B. Sadek, A. Ashoor, A. Siwek, M. Wiścek, K. Kucwaj, B. Filipiek, K. Kieć-Kononowicz, SAR-studies on the importance of aromatic ring topologies in search for selective 5-HT₇ receptor ligands among phenylpiperazine hydantoin derivatives, *Eur. J. Med. Chem.* 78 (2014) 324–339.
- K. Kucwaj-Brysz, D. Warszycki, S. Podlowska, J. Witek, K. Witek, A. González Izquierdo, G. Satala, M.I. Loza, A. Lubelska, G. Latacz, A.J. Bojarski, M. Castro, K. Kieć-Kononowicz, J. Handzlik, Rational design in search for 5-phenylhydantoin selective 5-HT₇R antagonists. Molecular modeling, synthesis and biological evaluation, *Eur. J. Med. Chem.* 112 (2016) 258–269.
- K. Kucwaj-Brysz, R. Kurczab, M. Jastrzębska-Więsek, E. Żesławska, G. Satala, W. Nitek, A. Partyka, A. Siwek, A. Jankowska, A. Wesolowska, K. Kieć-Kononowicz, J. Handzlik, Computer-aided insights into receptor-ligand interaction for novel 5-arylhydantoin derivatives as serotonin 5-HT₇ receptor agents with antidepressant activity, *Eur. J. Med. Chem.* 147 (2018) 102–114.
- K. Kucwaj-Brysz, R. Kurczab, E. Żesławska, A. Lubelska, M.A. Marć, G. Latacz, G. Satala, W. Nitek, K. Kieć-Kononowicz, J. Handzlik, The role of aryl-topology in balancing between selective and dual 5-HT₇/5-HT_{1A} actions of 3,5-substituted hydantoins, *Medchemcomm.* 9 (2018) 1033–1044.
- M. Leopoldo, E. Lacivita, F. Berardi, R. Perrone, P.B. Hedlund, Serotonin 5-HT₇ receptor agents: Structure-activity relationships and potential therapeutic applications in central nervous system disorders, *Pharmacol. Ther.* 129 (2011) 120–148.
- G. Latacz, A. Lubelska, M. Jastrzębska-Więsek, A. Partyka, K. Kucwaj-Brysz, A. Wesolowska, K. Kieć-Kononowicz, J. Handzlik, MF-8, a novel promising arylpiperazine-hydantoin based 5-HT₇ receptor antagonist: In vitro drug-likeness studies and in vivo pharmacological evaluation, *Bioorg. Med. Chem. Lett.* 28 (2018) 878–883.
- G. Latacz, A. Lubelska, M. Jastrzębska-Więsek, A. Partyka, A. Sobilo, A. Olejarsz, K. Kucwaj-Brysz, G. Satala, A.J. Bojarski, A. Wesolowska, K. Kieć-Kononowicz, J. Handzlik, In the search for a lead structure among series of potent and selective hydantoin 5-HT₇ R agents: The drug-likeness in vitro study, *Chem. Biol. Drug Des.* 90 (2017) 1295–1306.
- G. Koelsch, BACE1 Function and Inhibition: Implications of Intervention in the Amyloid Pathway of Alzheimer's Disease Pathology, *Molecules* 22 (2017) 1723.
- P.A. Dennery, Signaling function of heme oxygenase proteins, *Antioxid. Redox Signal.* 20 (2014) 1743–1753.
- R.K. Bunton-Stasyshyn, R.A. Saccon, P. Fratta, E.M. Fisher, SOD1 Function and Its Implications for Amyotrophic Lateral Sclerosis Pathology: New and Renascent Themes, *Neuroscientist* 21 (2015) 519–529.
- A.T. Dinkova-Kostova, P. Talalay, NAD(P)H:quinone acceptor oxidoreductase 1 (NQO1), a multifunctional antioxidant enzyme and exceptionally versatile cytoprotector, *Arch. Biochem. Biophys.* 501 (2010) 116–123.
- J. Kim, Y.N. Cha, Y.J. Surh, A protective role of nuclear factor-erythroid 2-related factor-2 (Nrf2) in inflammatory disorders, *Mutat. Res.* 690 (2010) 12–23.
- Q. Li, I.M. Verma, NF-kappaB regulation in the immune system, *Nat. Rev. Immunol.* 2 (2002) 725–734.
- A.P. Bento, A. Gaulton, A. Hersey, L.J. Bellis, J. Chambers, M. Davies, F.A. Krüger, Y. Light, L. Mak, S. McGlinchey, M. Nowotka, G. Papadatos, R. Santos, J. P. Overington, The ChEMBL bioactivity database: an update, *Nucleic Acids Res.* 42 (Database issue) (2014) D1083–D1090.
- B. Zdrzil, E. Felix, F. Hunter, E.J. Manners, J. Blackshaw, S. Corbett, M. de Veij, H. Ioannidis, D.M. Lopez, J.F. Mosquera, M.P. Magarinos, N. Bosc, R. Arcila, T. Kizilören, A. Gaulton, A.P. Bento, M.F. Adams, P. Monecke, G.A. Landrum, A.

- R. Leach, The ChEMBL Database in 2023: a drug discovery platform spanning multiple bioactivity data types and time periods, *Nucleic Acids Res.* 52 (2024) D1180–D1192.
- [45] X. Liu, C. Chen, C.E. Hop, Do we need to optimize plasma protein and tissue binding in drug discovery? *Curr. Top. Med. Chem.* 11 (2011) 450–466.
- [46] G. Xiong, Z. Wu, J. Yi, L. Fu, Z. Yang, C. Hsieh, M. Yin, X. Zeng, C. Wu, A. Lu, X. Chen, T. Hou, D. Cao, ADMETlab 2.0: an integrated online platform for accurate and comprehensive predictions of ADMET properties, *Nucleic Acids Res.* 49 (W1) (2021) W5–W14.
- [47] H. Yang, C. Lou, L. Sun, J. Li, Y. Cai, Z. Wang, W. Li, G. Liu, Y. Tang, admetSAR 2.0: web-service for prediction and optimization of chemical ADMET properties, *Bioinformatics* 35 (2018) 1067–1069.
- [48] F. Cheng, W. Li, Y. Zhou, J. Shen, Z. Wu, G. Liu, P.W. Lee, Y. Tang, admetSAR: a comprehensive source and free tool for assessment of chemical ADMET properties, *J. Chem. Inf. Model.* 52 (2012) 3099–3105.
- [49] S.K. Lee, G.S. Chang, I.H. Lee, J.E. Chung, K.Y. Sung, K.T. No, The PreADME: pc-based program for batch prediction of adme properties, *EuroQSAR* 9 (2004) 5–10.
- [50] D.E. Pires, T.L. Blundell, D.B. Ascher, pkCSM: Predicting Small-Molecule Pharmacokinetic and Toxicity Properties Using Graph-Based Signatures, *J. Med. Chem.* 58 (2015) 4066–4072.
- [51] E. Benfenati, A. Manganaro, G. Gini, VEGA-QSAR: AI inside a platform for predictive toxicology, *CEUR Workshop Proc.* 1107 (2013) 21–28.
- [52] Schrödinger Release 2023-3: QikProp, Schrödinger, LLC, New York, NY, 2023.
- [53] A. Daina, O. Michielin, V. Zoete, SwissADME: a free web tool to evaluate pharmacokinetics, drug-likeness and medicinal chemistry friendliness of small molecules, *Sci. Rep.* 7 (2017) 42717.
- [54] P. Banerjee, A.O. Eckert, A.K. Schrey, R. Preissner, ProTox-II: a webserver for the prediction of toxicity of chemicals, *Nucleic Acids Res.* 46 (W1) (2018) W257–W263.
- [55] A.A. Lagunin, V.I. Dubovskaja, A.V. Rudik, P.V. Pogodin, D.S. Druzhilovskiy, T. A. Glorizova, D.A. Filimonov, N.G. Sastry, V.V. Poroikov, CLC-Pred: A freely available web-service for in silico prediction of human cell line cytotoxicity for drug-like compounds, *PLoS One* 13 (2018) e0191838.
- [56] <http://predherg.labmol.com.br>; accessed on March 28th, 2024.
- [57] Y. Xu, Z. Dai, F. Chen, S. Gao, J. Pei, L. Lai, Deep Learning for Drug-Induced Liver Injury, *J. Chem. Inf. Model.* 55 (2015) 2085–2093.
- [58] A. Kaczor, J. Knutelska, K. Kucwaj-Brysz, M. Zygunt, E. Żesławska, A. Siwek, M. Bednarski, S. Podlowska, M. Jastrzębska-Więsek, W. Nitek, J. Sapa, J. Handzlik, The Subtype Selectivity in Search of Potent Hypotensive Agents among 5,5-Dimethylhydantoin Derived α_1 -Adrenoceptors Antagonists, *Int. J. Mol. Sci.* 24 (2023) 16609.
- [59] K. Witek, G. Latacz, A. Kaczor, J. Czekajewska, E. Żesławska, A. Chudzik, E. Karczewska, W. Nitek, K. Kieć-Kononowicz, J. Handzlik, Phenylpiperazine 5,5-Dimethylhydantoin Derivatives as First Synthetic Inhibitors of Msr(A) Efflux Pump in *Staphylococcus epidermidis*, *Molecules* 25 (2020) 3788.
- [60] Schrödinger Release 2023-3: LigPrep, Schrödinger, LLC, New York, NY, 2023.
- [61] D. Cao, J. Yu, H. Wang, Z. Luo, X. Liu, L. He, J. Qi, L. Fan, L. Tang, Z. Chen, J. Li, J. Cheng, S. Wang, Structure-based discovery of nonhallucinogenic psychedelics analogs, *Science* 375 (2022) 403–411.
- [62] S. Wang, T. Che, A. Levit, B.K. Shoichet, D. Wacker, B.L. Roth, Structure of the D2 dopamine receptor bound to the atypical antipsychotic drug risperidone, *Nature* 555 (2018) 269–273.
- [63] T. Asai, N. Adachi, T. Moriya, H. Oki, T. Maru, M. Kawasaki, K. Suzuki, S. Chen, R. Ishii, K. Yonemori, S. Igaki, S. Yasuda, S. Ogasawara, T. Senda, T. Murata, Cryo-EM Structure of K⁺-Bound hERG Channel Complexed with the Blocker Astemizole, *Structure* 29 (2021) 203–212.e4.
- [64] S. Sugio, A. Kashima, S. Mochizuki, M. Noda, K. Kobayashi, Crystal structure of human serum albumin at 2.5 Å resolution, *Protein Eng.* 12 (1999) 439–446.
- [65] Schrödinger Release 2023-3: Protein Preparation Wizard, Schrödinger, LLC, New York, NY, 2023.
- [66] Schrödinger Release 2023-3: Glide, Schrödinger, LLC, New York, NY, 2023.
- [67] Y. Cheng, W.H. Prusoff, Relationship between the inhibition constant (K_i) and the concentration of inhibitor which causes 50 per cent inhibition (I₅₀) of an enzymatic reaction, *Biochem. Pharmacol.* 22 (1973) 3099–3108.
- [68] R.L. Rich, Y.S. Day, T.A. Morton, D.G. Myszk, High-resolution and high-throughput protocols for measuring drug/human serum albumin interactions using BIACORE, *Anal. Biochem.* 296 (2001) 197–207.
- [69] P. Pyka, W. Haberek, M. Więcek, E. Szymanska, W. Ali, A. Cios, M. Jastrzębska-Więsek, G. Satala, S. Podlowska, S. Di Giacomo, A. Di Sotto, S. Garbo, T. Karcz, C. Lambona, F. Marocco, G. Latacz, S. Sudol-Talaj, B. Mordyl, M. Gluch-Lutwin, A. Siwek, K. Czarnota-Łydka, D. Gogola, A. Olejarz-Maciej, N. Wilczyńska-Zawal, E. Honkisz-Orzechowska, M. Starek, M. Dąbrowska, K. Kucwaj-Brysz, R. Fioravanti, M.J. Nasim, M. Hittinger, A. Partyka, A. Wesolowska, C. Battistelli, C. Zwergel, J. Handzlik, First-in-Class Selenium-Containing Potent Serotonin Receptor 5-HT₆ Agents with a Beneficial Neuroprotective Profile against Alzheimer's Disease, *J. Med. Chem.* 67 (2024) 1580–1610.
- [70] W. Ali, S. Garbo, A. Kincses, M. Nové, G. Spengler, E. Di Bello, E. Honkisz-Orzechowska, T. Karcz, E. Szymańska, E. Żesławska, M. Starek, M. Dąbrowska, W. Nitek, K. Kucwaj-Brysz, P. Pyka, R. Fioravanti, C. Jacob, C. Battistelli, C. Zwergel, J. Handzlik, Seleno-vs. thioether triazine derivatives in search for new anticancer agents overcoming multidrug resistance in lymphoma, *Eur. J. Med. Chem.* 243 (2022) 114761.